Received: 19 August 2020 | Revised: 5 February 2021 | Accepted: 9 February 2021

DOI: 10.1111/iar.12394

RESEARCH ARTICLE

Island Arc WILEY

Trace-element zoning patterns in porphyroblastic garnets in low-*T* eclogites: Parameter optimization of the diffusion-limited REE-uptake model

Ryo Fukushima[1] | Tatsuki Tsujimori[1,2] | Shogo Aoki[3,4] | Kazumasa Aoki[4]

[1]Graduate School of Science, Tohoku University, Sendai, Japan

[2]Center for Northeast Asian Studies, Tohoku University, Sendai, Japan

[3]Graduate School of International Resource Sciences, Akita University, Akita, Japan

[4]Center for Fundamental Education, Okayama University of Science, Okayama, Japan

Correspondence
Ryo Fukushima, Graduate School of Science, Tohoku University, 41 Kawauchi, Aoba, Sendai 980-8576, Japan.
Email: ryo.fukushima.p7@dc.tohoku.ac.jp

Funding information
Japan Society for the Promotion of Science, Grant/Award Numbers: JP15H05212, JP18H01299, JP19K04043

Abstract

Compositional zoning patterns of the major elements and REEs in prograde-zoned garnets whose Mg/(Mg + Fe) atomic ratios increase rimward have been widely used to understand the metamorphic *P*–*T*–*t* trajectories, and the diffusion-limited REE-uptake model is a promising way to interpret their growth rates and the REE diffusion kinetics in the low-temperature eclogite. In order to elucidate their growth kinetics with Skora et al.'s (2006) diffusion-limited REE uptake model for prograde-zoned garnets, we examine the trace-element zoning patterns of two prograde-zoned porphyroblastic garnets (~6 mm in size) in low-temperature eclogites from two different localities. Core-to-rim trace-element profiles in a garnet (prp_{5-9}-$alm_{61-67}sps_{1-3}grs_{24-30}$) of a glaucophane-bearing epidote eclogite of Syros (Cyclades, Greece) are characterized by the presence of Y + HREE peaks in the mantle, which might be attributed to a continuous breakdown of the titanite to form rutile during the garnet growth. In contrast, those in a garnet ($prp_{4-7}alm_{61-68}$-$sps_{3-10}grs_{23-24}$) extracted from a lawsonite-eclogite of the South Motagua Mélange (SMM) (Guatemala) have prominent central peaks of Y + HREEs. Although the REE profiles of both the garnets can be explained by the diffusion-limited uptake, their Mn profiles suggest that their growth-rate laws are different: i.e., diffusion-controlled (Syros) and interface-controlled (SMM). Prior to the model application, we optimize the number of the parameters as the garnet grows with the interface-controlled processes based on the growth Péclet number. In particular, we propose the ratio of the REE diffusivity in the eclogitic matrix to the garnet growth rate as the new parameter. Visualizing the values of the new parameters allows to readily understand the relationship between the REE profiles and the REE-diffusion/garnet-growth kinetics in low-*T* eclogite. Our model refinement leads to the simple quantitative characterization of core-to-rim REE profiles in garnet in low-temperature eclogites.

KEYWORDS
diffusion-limited REE uptake model, eclogite, growth kinetics, zoned garnet

1 | INTRODUCTION

Garnet in metamorphic rocks has received considerable attention because of its common occurrence and its major/rare-earth element (REE) zoning in rocks recrystallized under various pressure–temperature (*P*–*T*) conditions (cf., Baxter et al., 2013, 2017). Because of the limited scale of cation diffusion, strong compositional zoning patterns are often observed at low temperature. For example, below ~600 °C, the diffusion lengths of divalent cations in garnet are estimated to be up to ~100 μm (Caddick et al., 2010). Considering a garnet whose radius is a few millimeters, the diffusion lengths are a few percent of the radius at the most, which means the zoning has been almost preserved. This characteristic feature enables us to unravel the history of the low- to moderate-*T* metamorphism. Focusing on very slow intracrystalline diffusion in garnet and mineral inclusions enclosed in it, many researchers have discussed *P*–*T* trajectories based on the zoned garnet (e.g., Banno & Chii, 1978; Carlson, 2012; Enami et al., 2007; Fukushima et al., in press; Inui & Toriumi, 2004; Kohn et al., 1993; Konrad-Schmolke et al., 2005; Sakai et al., 1985; Skora et al., 2006; Spear & Selverstone, 1983).

Prograde-zoned garnet is also the key to revealing the crystallization kinetics of the regional metamorphism. Thus far, several studies have tried to estimate growth rates of the porphyroblastic garnets (e.g., Christensen et al., 1989; Lapen et al., 2003; Pollington & Baxter, 2010). Garnet geochronology based on the radioisotope systems, such as Sm–Nd, Rb–Sr, and Lu–Hf, not only can constrain growth timings of garnets but also might provide their core-to-rim time intervals, namely, the growth duration. For example, using the Rb–Sr isotopic system, Christensen et al. (1989) estimated the average growth rate of garnets (~3 cm in size). Specifically, they chose two different segments from the core and the rim of a single garnet to date. They found the garnets had grown by $\sim 1.4 \times 10^{-7}$ cm·yr^{-1}. Pollington and Baxter (2010) determined a radius–time path based on 12 Sm–Nd isotope analyses on a single zoned-garnet (~6 cm in size). They found that its total growth span was ~7.55 Myr though its growth was characterized by two distinct pulses of accelerated growths. Lapen et al. (2003) applied multiple isotopic systems and tried to estimate garnet growth rates. They pointed out that bulk garnet ages obtained from the Lu–Hf and the Sm–Nd isotopic systems were different due to the difference of the zoning patterns of Lu and Sm. Using the age difference, they estimated garnet growth duration in a certain metamorphism. Kohn (2009) also applied the same approach and showed that the age difference between the isotope systems reached up to 30 % of the total growth duration. Nevertheless, no appropriate technique has yet been established to estimate a growth rate of a certain mm-size garnet at low temperature. If we succeed in obtaining kinetic data from such garnet in natural metamorphic rocks, we can understand not only the timescale of the whole metamorphism but also the individual geological events recorded in the metamorphic rocks, such as the fluid-mediated garnet growth.

Another potential approach to constrain the garnet growth rate is characterizing the chemical zoning of prograde-zoned garnets. Skora et al. (2006) proposed a garnet-zoning model based on the diffusion-limited REE uptake. With Skora et al.'s model, we can replicate REE zoning patterns in natural garnet porphyroblasts by setting various parameters including their growth duration. However, it is still difficult to estimate garnet-growth duration based on its REE profiles, because we cannot determine the genuine parameter set based only on the profile with a one-to-one correspondence. If we could solve this problem, the uptake model would be a promising tool to clarify the garnet-growth histories.

In this paper, we examine the compositional zoning patterns for the major/trace elements of two single porphyroblastic garnets in low-temperature eclogites from two different metamorphic terranes (Syros and the South Motagua Mélange [SMM]) as preliminary challenges for elucidating their growth kinetics. To achieve this objective, we propose a new way of interpreting Skora et al.'s model with the aim of determining the parameter sets with a one-to-one correspondence.

2 | GEOLOGICAL OUTLINES AND SAMPLE DESCRIPTIONS

We examined two euhedral porphyroblastic garnets: S01 and G01, extracted from a glaucophane-bearing epidote eclogite in Cycladic Blueschist Unit, Syros, Greece and a lawsonite eclogite in the SMM, Guatemala, respectively. Both of them are moderate to large in size (~6 mm in diameter) and rhombic dodecahedrons in shape, having 12 crystallographic equivalent {110} planes.

2.1 | Geological outlines

2.1.1 | Garnet S01—Syros (Cyclades, Greece)

Syros Island, which belongs to Cyclades Archipelago, is located at the center of the Aegean domain. Its lithological sequence consists mainly of alternating marbles and H*P* schists, which are part of the Cyclades Blueschist Unit (CBU). Cyclades Archipelago is the deepest exhumed parts of the belt and its peak-pressure conditions were achieved at ~53–48 Ma (Lagos et al., 2007; Lister & Forster, 2016; Tomaschek et al., 2003; Uunk et al., 2018). The peak metamorphic *P*–*T* condition of the CBU and its *P*–*T* path were estimated by many workers (Laurent et al., 2018; Lister & Forster, 2016; Schumacher et al., 2008; Trotet et al., 2001). All of the estimated paths are clockwise, and the retrograde paths are characterized by nearly isothermal decompression. The peak metamorphic condition of the CBU on Syros is obtained at ~500–560 °C and ~2.2–2.4 GPa (Laurent et al., 2018), while Schumacher et al. (2008) suggested a lower condition at ~500 °C and ~1.5–1.6 GPa.

The CBU in Syros contains dismembered meta-ophiolite, whose protoliths were derived from altered oceanic crust (Seck et al., 1996). In Syros, the CBU was divided into three subunits (Laurent et al., 2016): Posidonia, Chrousa, and Kampos Subunits, in structurally ascending order from the bottom to the top. The investigated sample

was obtained from the Kampos Subunit, which is a tectonic mélange of metabasites and eclogite.

2.1.2 | Garnet G01—The SMM (Guatemala)

The Motagua Suture is a fault-bound region in central Guatemala, where the North American–Caribbean plate boundary is located (e.g., Harlow et al., 2004). The SMM is an eclogite- and blueschist-bearing mélange unit, located at the south of the Motagua Suture. The SMM is well known for the occurrence of jadeitite and lawsonite eclogite (Brueckner et al., 2009; Harlow et al., 2004; Tsujimori et al., 2005, 2006a, 2006b; Tsujimori & Ernst, 2014). Lawsonite eclogites of the SMM are categorized into L-type lawsonite eclogites (Hara et al., 2018; Tsujimori et al., 2006a; Tsujimori & Ernst, 2014), which means that prograde-zoned garnet grew within the lawsonite stability field. Lawsonite inclusions within garnet contain rare pumpellyite. The prograde eclogite metamorphism was estimated to have occurred at ~480 °C and ~2.4–2.6 GPa (Tsujimori et al., 2006b). Sm–Nd mineral isochrons from the lawsonite eclogites yield 143.9–132.1 Ma (Brueckner et al., 2009). The investigated sample was collected in the Carrizal Grande; details are referred to Tsujimori et al. (2005, 2006a, 2006b).

2.2 | Sample descriptions

2.2.1 | Syros eclogite (glaucophane–epidote eclogite)

The Syros sample (Figure 1a) is a foliated glaucophane–epidote eclogite. It contains euhedral garnet porphyroblasts (~3–6 mm in size) distributed in an omphacite-dominant foliated matrix (Figure 1c). The matrix-forming minerals are columnar/needle-like omphacite (typically ~100–200 μm in length) and phengitic white mica (typically ~100–1000 μm in length). The matrix also contains minor amounts of glaucophane, clinozoisite, rutile, quartz, apatite and secondary albite. Some of the matrix rutile crystals occur as pseudomorphs after titanite. The garnet porphyroblasts contain omphacite, clinozoisite and rutile; rutile tends to be scattered over the garnet rims, rather than on their cores (Figure 1c,d). In some cases, inclusion trails of omphacite and clinozoisite parallel to the matrix foliation are found in the garnets (Figure 1d).

S01, the largest porphyroblastic garnet in the hand-sized specimen (Figure 1b), contains abundant mineral inclusions (typically ~10–100 μm in size), mainly of omphacite ($jd_{\sim 40-50}$) and clinozoisite [$Fe^{3+}/(Fe^{3+} + Al)$ atomic ratio = ~0.2]. Omphacite occurs as irregularly rounded anhedral crystals. The garnet crystal also contains minor amounts of rutile, titanite, carbonate, apatite, chlorite, quartz, paragonite, jadeite ($jd_{\sim 95}$), zircon. Titanite tends to occur as primary inclusions at the garnet core, while titanite replaces primary rutile inclusions along micro cracks in the mantle and rim. Chlorite and albite are also found as secondary replacements of primary inclusions along the microcracks.

2.2.2 | SMM eclogite (lawsonite eclogite)

The investigated sample is a Type-I eclogite of Tsujimori et al. (2006b), containing mm-sized euhedral garnets within a weakly foliated matrix. The matrix is characterized by recrystallized omphacite and lawsonite, with minor secondary chlorite, titanite, phengite, and quartz.

The extracted garnet (G01) is the largest crystal in a hand specimen. G01 contains abundant inclusions (typically ~10–100 μm in size) of omphacite ($jd_{\sim 35-60}$), jadeite ($jd_{\sim 80-90}$), lawsonite and minor amounts of rutile and quartz. Tiny zircons, phengite, allanite, and secondary titanite and albite after jadeite are also included.

3 | ANALYTICAL PROCEDURES

3.1 | Sample fabrication

To characterize the core-to-rim compositional zoning of the extracted garnets, we firstly measured the distance between their opposite

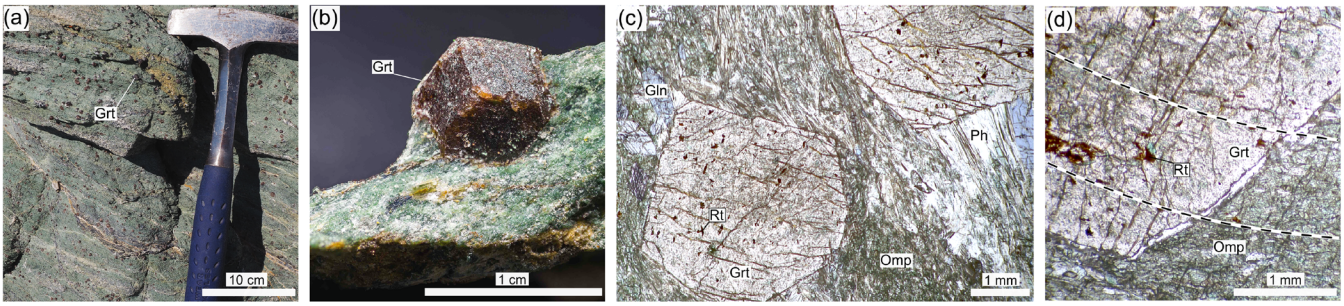

FIGURE 1 Images of the investigated Syros eclogite: (a) low-*T* eclogite in Syros showing abundant garnet porphyroblasts in a foliated matrix; (b) the S01 garnet; (c) photomicrograph of the eclogite which shows garnet porphyroblasts and the foliated matrix; (d) photomicrograph of a garnet porphyroblast which contains omphacite inclusion trails along the foliation (dashed lines). Grt, garnet; Gln, glaucophane; Omp, omphacite; Ph, phengite; Rt, rutile

crystal planes, and then cut each of the extracted garnet at nearly its center. After mounting the garnet with epoxy resin, we carefully polished it to observe the garnet core using a Maruto Prepalap MG-300 stepwise controllable polisher.

3.2 | Petrographic observations and EDS analysis

The polished samples were observed using a JEOL JSM-7001F field emission-scanning electron microscope (FE-SEM) at Tohoku University. For the petrographic observation by FE-SEM, the back-scattered electron (BSE) imaging was performed at a 15 kV acceleration voltage and a 3 nA beam current. Furthermore, X-ray maps for Mg, Al, Ca, Fe, and Mn were obtained using a JEOL JXA-8200 wavelength-dispersive electron microprobe analyzer at Bayerishes Geoinstitut, with an acceleration voltage 15 kV and a current of 500 nA.

The major element compositions of garnets and their inclusions were analyzed by a Hitachi S-3400N SEM, equipped with an energy dispersive X-ray spectrometry (EDS), Oxford INCA X-act energy dispersive X-ray spectrometers. The acceleration voltage and beam current were maintained at 15 kV and 1 nA, respectively.

3.3 | Trace element analyses

Rim-core-rim profiles of the major and trace elements (Li, Na, Mg, Al, Si, P, K, Ca, Ti, Mn, Fe, Sr, Y, Zr, La, Ce, Pr, Nd, Sm, Eu, Gd, Tb, Dy, Ho, Er, Tm, Yb, Lu, and Hf) were characterized by using a Thermo Scientific iCAP RQ inductively coupled plasma quadrupole mass spectrometry (ICPQMS) coupled to Teledyne Analyte G2 laser ablation (LA) system that uses a 193 nm excimer laser (laser settings: 7 Hz, fluency 13.20 $J \cdot cm^{-2}$, spot size 5 μm square) in the Okayama University of Science. Raster (line scan) analysis moving the sample cell of the LA system at a speed of 5 $\mu m \cdot s^{-1}$ was adopted in order to get signals easily from as many points on the garnets as possible, not on their inclusions. NIST SRM 610 glass (Pearce et al., 1997) was used as an external standard. Each integration time at the ICP-MS analysis was set to 0.05 s for ^{7}Li and ^{178}Hf, 0.01 s for ^{23}Na, ^{24}Mg, ^{27}Al, ^{29}Si, ^{31}P, ^{39}K, ^{44}Ca, ^{49}Ti, ^{55}Mn, and ^{56}Fe, 0.03 s for ^{88}Sr, ^{89}Y, ^{90}Zr, and ^{139}La, 0.08 s for ^{140}Ce, ^{141}Pr, ^{146}Nd, and ^{147}Sm, and 0.04 s for ^{153}Eu, ^{157}Gd, ^{159}Tb, ^{163}Dy, ^{165}Ho, ^{166}Er, ^{169}Tm, ^{172}Yb, and ^{175}Lu (meaning that the signal data were output every second). The line profiles of their elements were calculated as oxide by normalizing total component percentages to 100 % using the software iQuant2 (Suzuki et al., 2018). The raster analyses of the reference garnet (GA1, Fukuyama et al., 2007) indicate that the averages of each of the middle/heavy REE (MREE/HREE) concentrations (∼3–30 $\mu g \cdot g^{-1}$) obtained from a few adjacent points have the errors of <∼30 % on a relative basis. Although the obtained profiles often include noise associated with the measurement process, their intensities seem to be almost within the errors. In fact, the REE concentrations of the reference garnet were homogeneous within the error. Hence, this analytical method is reasonable to grasp the overall trends of the REE profiles. We eliminated the effects of the inclusions as follows. Firstly, signals of some included minerals (clinopyroxene, zircon, apatite, rutile, and titanite) are excluded by setting certain thresholds: 0.1 wt% (Na_2O, ZrO_2), 0.3 wt% (TiO_2), and 1 wt% (P_2O_5). Then, based on measured atomic ratios of divalent cations to Si and Al, we chose signals from the garnets in terms of stoichiometry. In addition, when irregular signals due to mineral inclusions were seen in major-element profiles, we excluded all signals from the points as failure. In Document S1, we show our program code in R 3.6.0 for this procedure.

4 | RESULTS

4.1 | Syros garnet (S01)

4.1.1 | Major elements

S01 has an almandine-rich composition ($prp_{5-9}alm_{61-67}sps_{1-3}grs_{24-30}$) and exhibits a concentric zoning pattern, where Mg# = Mg/(Mg + Fe) roughly increases rimward and Mn decreases from the core to the mantle (Figure 2). The Ca profile slightly increases rimward. Notably, a discontinuous, rimward Mn-enrichment is found at the rim (upper side of Figure 2; white arrow). Considering the too low metamorphic temperatures (<∼550 °C) for the divalent cations to diffuse within garnet (e.g., Caddick et al., 2010), this enrichment is attributed to abrupt Mn supply into the growing garnet rim, or a pause/acceleration in the garnet growth followed by a change in Mn-diffusive flux into the garnet. The outside of the discontinuity is characterized by a spike of Ca–Mn enrichments. Locally, we observe another Mn spike at the very edge of the garnet, which is probably due to the secondary Mn uptake which occurs synchronously with a slight resorption of the garnet (e.g., Banno & Chii, 1978; Kim, 2006).

4.1.2 | Trace elements

Trace-element profiles of S01 are shown in Figure 3. To compare the distributions of some trace-element spikes to the major-element profiles, the MnO profiles are also shown. Since there are no minerals containing MnO in the wt% order other than garnet in both of the eclogites (see Section 2.2), the Mn profiles would be directly affected by the garnet-growth histories during the eclogitization. For the Sm profile, we cannot detect any clear zonation. Generally, due to their high partitioning behavior into garnet, natural garnets are often characterized by sharp rimward decreases of MREE–HREE–Y concentrations from the core (e.g., Hickmott & Shimizu, 1990; Raimondo et al., 2017); we define this type as 'A-shaped' profiles. However, there are no such A-shaped profiles in S01. The Eu and Gd profiles show acute peaks at the garnet core (∼5 and ∼25 $\mu g \cdot g^{-1}$, respectively) and weak secondary peaks at the mantle (∼2 and ∼10 $\mu g \cdot g^{-1}$, respectively). Most of the profiles except for Eu and Gd seem to have high concentration from the mantle to rim, which are similar to the 'M-shaped' profiles in Skora et al. (2006). Although the Sm profile has

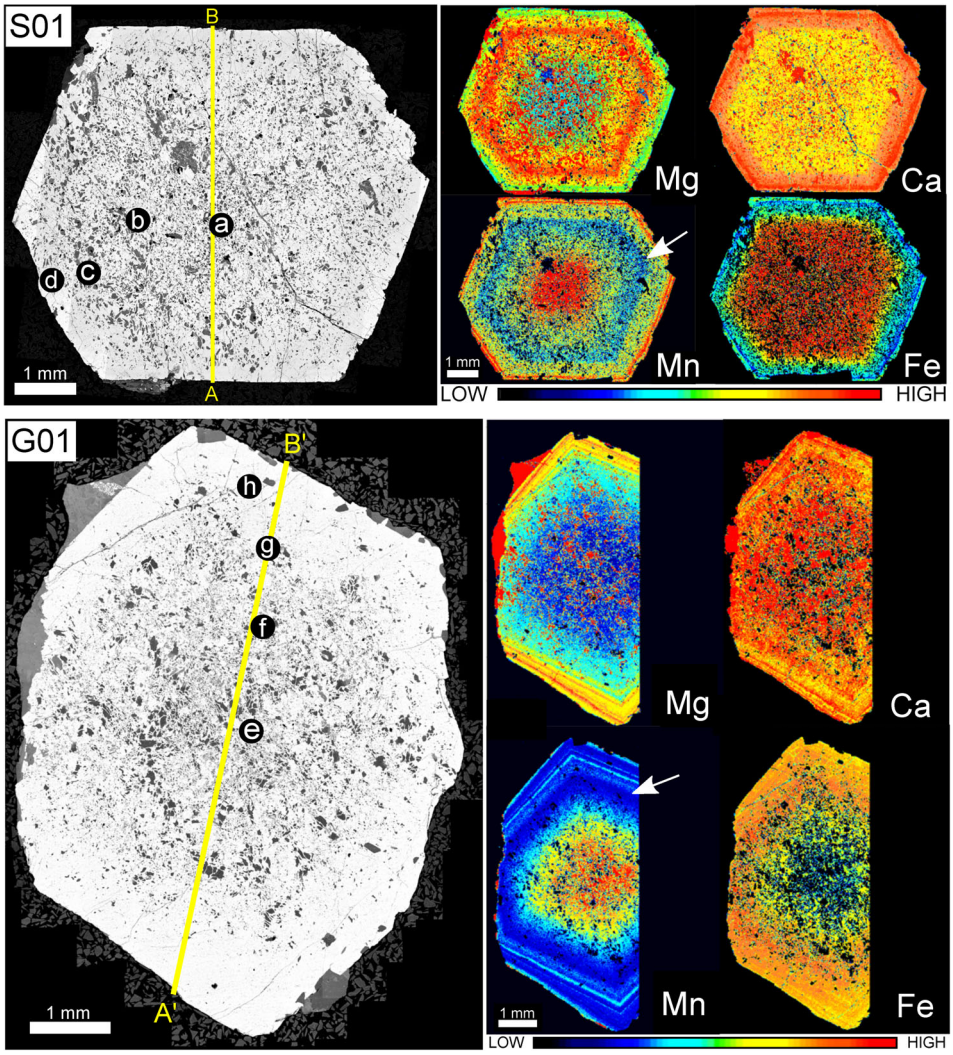

FIGURE 2 BSE images and major-element X-ray maps of the S01 (upper) and the G01 (lower) garnets. Along the yellow lines in the BSE images, we measured line profiles of elements including Y + HREEs (Figures 3 and 4). The white arrows indicate compositional discontinuities observed in both of the Mn profiles. The representative major-element compositions are:
(a) $prp_5alm_{67}sps_3grs_{24}$;
(b) $prp_6alm_{67}sps_2grs_{25}$;
(c) $prp_9alm_{66}sps_1grs_{25}$;
(d) $prp_8alm_{61}sps_2grs_{30}$;
(e) $prp_4alm_{61}sps_{10}grs_{24}$;
(f) $prp_4alm_{64}sps_7grs_{24}$;
(g) $prp_7alm_{68}sps_3grs_{23}$;
(h) $prp_7alm_{65}sps_4grs_{24}$

the major modes at the rim (~2–3 $\mu g \cdot g^{-1}$), the other M-shaped profiles have the peaks at the mantle (Tb ~4–7 $\mu g \cdot g^{-1}$; Dy ~60 $\mu g \cdot g^{-1}$; Ho ~20 $\mu g \cdot g^{-1}$; Y ~ 600 $\mu g \cdot g^{-1}$; Er ~60–80 $\mu g \cdot g^{-1}$; Tm ~11–13 $\mu g \cdot g^{-1}$; Yb ~60–110 $\mu g \cdot g^{-1}$; Lu ~5–15 $\mu g \cdot g^{-1}$). Exceptionally, the Lu profile also has a prominent peak at the core (~15 $\mu g \cdot g^{-1}$).

The M-shaped peaks and the Eu–Gd secondary peaks are located at the distance of ~0.1–0.2 cm and ~0.3–0.5 cm from the rim_A. Especially, most of the M-shaped profiles are characterized by steep drops in their concentrations at the distance of ~0.2 and ~ 0.4 cm from the rim_A. Although Skora et al. (2006) reported the shift of secondary peaks towards the garnet rim with decreasing atomic number for REEs, in this case we cannot observe the trend clearly. It is also different from the result of Skora et al. (2006) that the shapes of our Y and HREE profiles are not highly symmetric.

Despite the discordance among the profiles, the Y and HREE profiles have a common trend specifically outside the Mn discontinuity; most of them are characterized by slight enrichments at the Mn discontinuity and by relatively large spikes at the edge of the garnet. These acute enrichments seem to be concordant with the Mn spike. We frequently observe this trend at the portion closer to the rim_B rather than the other. Nevertheless, it is uncertain whether this asymmetric feature is due to analytical obstacles or actual heterogeneous distributions of the spikes. Specifically, around the rim_B, there are various measurement points of garnet, not being interrupted by the mineral inclusions. On the other hand, the other portion has only five signals from the garnet, which leads to uncertainty about the interpretation of the Y + HREE spike distributions at the garnet rim.

4.2 | SMM garnet (G01)

4.2.1 | Major elements

G01 is also characterized by an almandine-rich composition ($prp_{4-7}alm_{61-68}sps_{3-10}grs_{23-24}$) with a concentric zoning pattern, where the Mg# roughly increases rimward and Mn concentration decreases from the core to the rim (Figure 2). It also has a discontinuous, rimward Mn enrichment at the rim (lower side of Figure 2; white arrow). However, differently from S01, the Ca concentration in G01 is homogeneous. Moreover, the G01 rims outside the Mn discontinuity can be distinguished from the inside portion in their (1) oscillatory compositional zoning; (2) few mineral inclusions; and (3) anisotropic spatial

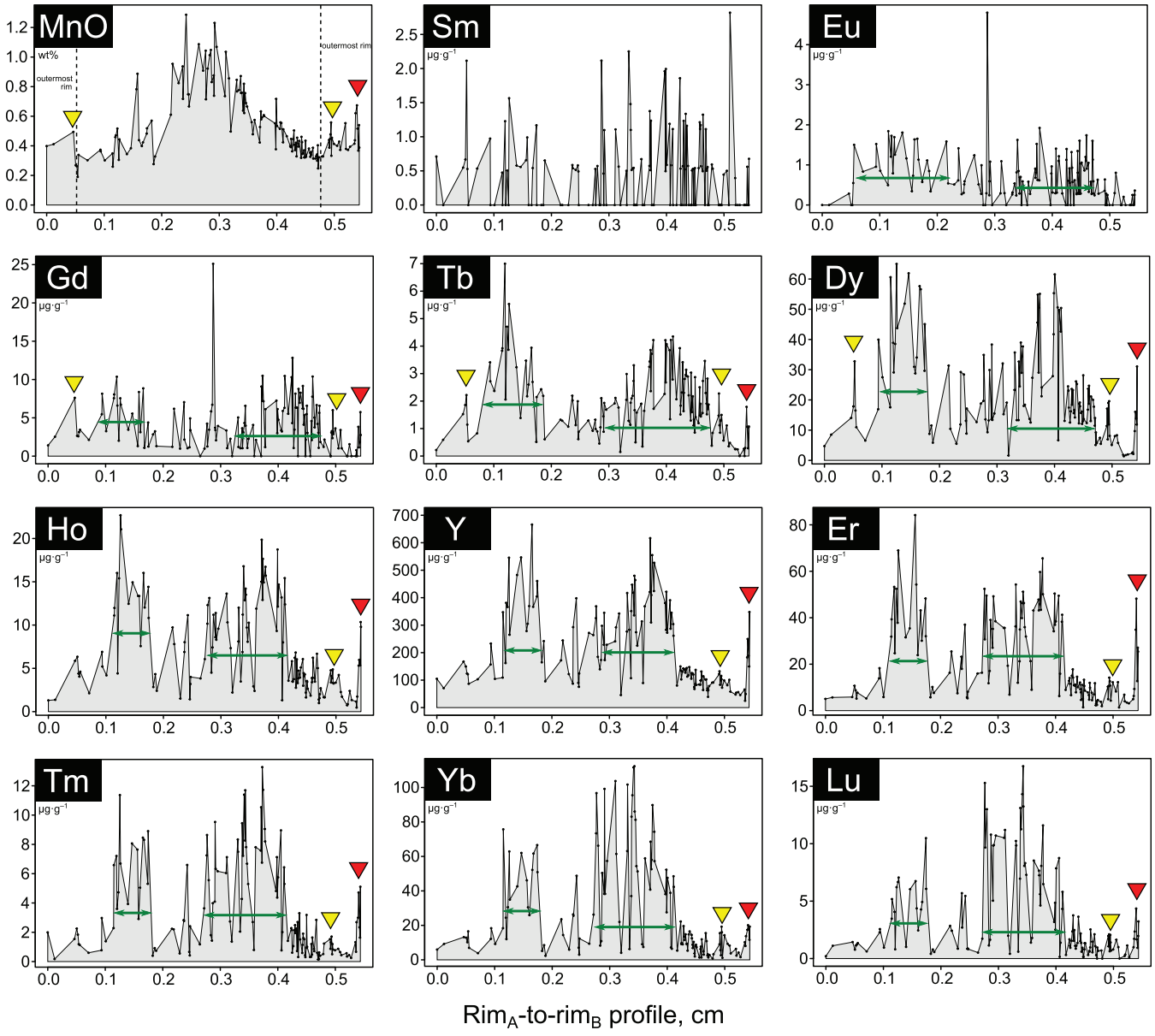

FIGURE 3 Line profiles of Y + HREEs in the S01 garnet. MnO, Sm and Eu profiles are also shown. The yellow and red marks indicate the compositional discontinuities and the enrichments at the garnet edge, respectively. The green arrows indicate the ranges of the secondary peaks

distribution. These peculiar characteristics suggest that the G01 rims outside the Mn discontinuity formed during a different metamorphic event from that for the inside of the discontinuity. Considering the presence of the oscillatory zoning, we can assume that the G01 rims outside the discontinuity overgrew in fluid-dominated environments (e.g., Yardley et al., 1991). Nevertheless, like S01, the overgrown rim is characterized by two major Mn spikes, including that probably due to the resorption-induced Mn uptake at the very edge of the garnet.

4.2.2 | Trace elements

G01 has both of the A-shaped type (Tm, Yb, Lu) and the M-shaped type (Sm) profiles (Figure 4), which resembles the result of Skora et al. (2006). As with S01, the Eu and Gd profiles have acute peaks at the garnet core (~5 and ~25 $\mu g \cdot g^{-1}$, respectively) and secondary peaks at the rim (~4 and ~15–20 $\mu g \cdot g^{-1}$, respectively). The Tb, Dy, Ho, Y, and Er profiles are apparently like A-shaped but they have weak secondary peaks at the rim. The A-shaped and these apparently A-shaped profiles are characterized by prominent spikes at the core: Tb ~15 $\mu g \cdot g^{-1}$; Dy ~200 $\mu g \cdot g^{-1}$; Ho ~80 $\mu g \cdot g^{-1}$; Y ~ 2000 $\mu g \cdot g^{-1}$; Er ~250 $\mu g \cdot g^{-1}$; Tm ~60 $\mu g \cdot g^{-1}$; Yb ~400 $\mu g \cdot g^{-1}$; Lu ~40 $\mu g \cdot g^{-1}$. The M-shaped Sm profile has spikes at the rim (~6–8 $\mu g \cdot g^{-1}$).

Notably, all of the rim spikes mentioned above are located in the overgrown area. Specifically, the secondary peaks of the apparently A-shaped profiles correspond to one of the major Mn enrichments closer to the core. Moreover, these profiles have prominent signals at the very edge of the garnet, which is concordant with the resorption-

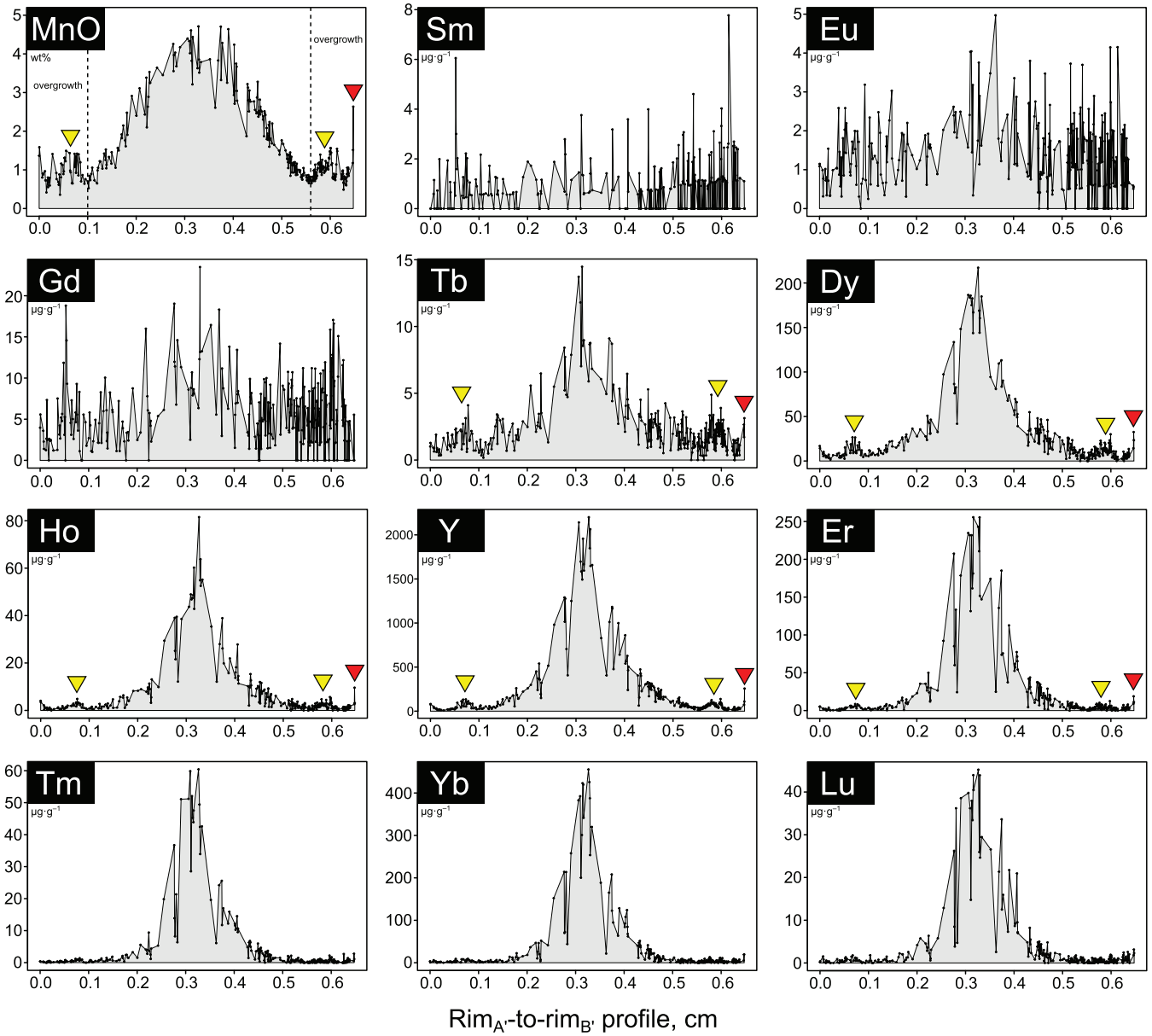

FIGURE 4 Line profiles of Y + HREEs in the G01 garnet. MnO, Sm and Eu profiles are also shown. The yellow and red marks indicate the compositional discontinuities and the enrichments at the garnet edge, respectively

induced Mn enrichment. As for the Eu and Gd profiles, though their secondary peaks are located at the outside rim, their shapes do not resemble the Mn enrichments. Although the intensities of the outermost Y–HREE–Mn enrichments are not necessarily equal between the $rim_{A'}$ and $rim_{B'}$, all outlines of the trace-element profiles in G01 are symmetric like the result of Skora et al. (2006).

5 | VALIDITY OF THE TRACE-ELEMENT PROFILE MEASUREMENTS

In order to properly describe the REE-uptake processes in each of the garnets, we have to measure its REE profiles so that they can include signals from the center of the garnet. The nearly symmetric trace-element profiles with the steep core enrichments of Y + HREEs in G01 indicate that we succeeded in measuring the G01 trace-element profiles with the center-identification. Although the overgrown rims of G01 contain asymmetric Y–HREE–Mn spikes, it does not necessarily mean that our measurements are inappropriate. This is because these spikes would have formed with the resorption-induced elemental uptake, and because the garnet-resorption process can occur spatially heterogeneously. On the other hand, however, we cannot readily confirm that the S01 trace-element profiles rigorously include such center-derived signals due to their complicated, asymmetric shapes.

To interpret the S01 profiles, we focus on the point that the profiles except for Sm have peaks at the mantle of the garnet and we

cannot observe their rimward shifts according to the atomic-number decrease of the REE. We cannot explain this characteristic without external controls on the Y + HREE content in the bulk system such as the breakdown of HREE-rich minerals. One of the most possible candidates is titanite because it is known to incorporate more Y + HREE content than rutile (e.g., Tribuzio et al., 1996). In fact, the S01 core contains titanite as primary inclusions. The breakdown of titanite-bearing mineral assemblages to form rutile during the S01 growth is a reasonable scenario to explain the steep increase of Y + HREEs at the mantle of the garnet. If this interpretation is correct, the steep drops in Tb–Lu concentrations at the distance of ~0.2 and ~0.4 cm from the rim_A would be attributed to the beginning and end of the titanite breakdown. Besides, the S01 trace-element profiles are asymmetric except for Eu and Gd. This indicates that the titanite crystals were heterogeneously distributed in the matrix during the prograde stage, and that the Eu and Gd profiles were little affected by the external modification. The acute central peaks of Eu and Gd should therefore be the signals from the genuine garnet core, not due to the external REE infiltration. Hence, we conclude that the trace-element profiles of each of the garnets include signals from the genuine garnet core. Nevertheless, due to the presence of titanite, most of the REE profiles in S01 are inappropriate for the REE-uptake analyses with the previous model.

6 | DISCUSSION

6.1 | Diffusion-limited REE-uptake model based on Skora et al. (2006)

We herein evaluate the obtained trace-element profiles and discuss the REE-uptake in the garnets. We wrote a program code in R 3.6.0 to package it as a diffusion-limited REE uptake simulator 'dluskora' (https://github.com/Ryo-fkushima/dluskora). This is based on the diffusion-limited REE uptake model by Skora et al. (2006). Prior to applying the model to the natural samples, we describe the model in detail.

The Skora et al.'s model is a method of solving trace-element partitioning problems between a growing crystal and the matrix, especially for the diffusion-limited REE uptake by prograde-zoned garnet in the low-*T* eclogite. Since one cannot solve the problem with a finite reservoir explicitly, they proposed a numerical method based on the Crank–Nicholson scheme (Crank, 1975). This model is useful for explaining the complex REE zoning patterns in garnet, and was reappraised by Hesse (2012), Moore et al. (2013), and Tan et al. (2020). This model can be applied to the low-*T* conditions under which REE diffusion around a given garnet is too slow to maintain equilibrium and REE diffusion in the garnet can be neglected. Since both of the metamorphic peak temperatures of our samples are estimated to be distinctly lower than 600 °C, this application should be reasonable.

The model system is composed of a sphere of fixed size which a garnet nucleates and grows at the center of. The garnet is approximated by a spherical crystal growing radially. The sphere is filled with a continuum containing an average initial REE concentration. To describe the condition above, we first used Fick's second law in the spherical coordinate system:

$$\frac{\partial C}{\partial t} = D\frac{\partial^2 C}{\partial r^2} + \frac{2D}{r}\frac{\partial C}{\partial r}, \quad (1)$$

where C is the REE concentration around the garnet, D is the effective diffusion coefficient, r is the radius, and t is the time. Notably, the unique characteristic of the model is that the REE diffusion coefficients around the garnet increase according as temperature increases; they follow the Arrhenius equation, $D_{(t)} = D_0 \exp(-Q/RT_{(t)})$, where D_0 is the pre-exponential factor, Q is the activation energy, R is the universal gas constant, and T is temperature. Then, discretizing Equation (1), we solved the diffusion equation numerically. A no flux boundary condition was applied at the outermost boundary of the system. The left-side boundary was the moving garnet–matrix interface, whose distance from the garnet core increases with time. The garnet radius was expressed as:

$$r_{Grt} = \alpha t^f, \quad (2)$$

where r_{Grt} is the growing garnet radius, t is the time, and f is the exponent of the garnet-growth rate law. When $f = 1$, the garnet radius is a linear function of time and α is regarded as the garnet growth rate. The rim composition of the newly grown garnet is calculated on the basis of the constant partition coefficient (K), so that the mass balance of REE flux around the garnet can be retained.

Setting the following parameters, we can estimate certain REE profiles with this model: D_0, α, Q, K, the radius of the system (R_{sys}), the final radius of the garnet (R_{gar}), the average initial REE concentration (C_{ave}), the initial/final temperatures (T_1/T_2), and the exponents of the garnet-growth/temperature-increase laws (f/f_T) (Table 1). We also need to set the number of the time and the spatial steps for the numerical calculation. To evaluate whether the numbers of the time/spatial steps are appropriate, we calculated the overall mass balance every time step; we chose the proper conditions so that the overall net mass gain could not exceed 0.01 % of the total REE content in the spherical system.

6.2 | Determination of the growth- and uptake-rate laws

For sophisticated analyses of garnet growth with the REE uptake, we should fix the function form of the growing garnet radius, the f value, in advance. Traditionally, the function form has been approximated on the basis of the rate-limiting process of the garnet growth. If a given garnet porphyroblast grows with the interface-controlled process, its radius is approximated by a linear function of time ($f = 1$), while if a given garnet porphyroblast grows with the diffusion-controlled process, its growth is defined as the square root of time growth rate law

TABLE 1 Parameters required for the diffusion-limited REE uptake modeling

Parameters	Descriptions	Parameter treatments in this study
D_0	the pre-exponential factor of the REE diffusion coefficient in the eclogitic matrix	integrated into the new variable u (= D_0/α)
α	the garnet growth rate ($r = \alpha t^f$)	ditto
Q	the activation energy of the REE diffusion coefficient in the eclogitic matrix	variable
K	the REE partition coefficient (Grt/matrix)	adjusted to the values which explain the central REE peaks
R_{sys}	the radius of the system sphere	variable
R_{gar}	the final radius of the garnet	fixed (measured)
C_{ave}	the initial REE concentration in the system	fixed (measured)
T_1, T_2	the initial/final temperatures during the garnet growth	fixed (estimated)
f	the exponent of the garnet-growth law ($r = \alpha t^f$)	fixed to 1
f_T	the exponent of the temperature-increase law ($T \propto t^{f_T}$)	fixed to 2
M_t	the number of the time steps	adjusted so that the overall net mass gain cannot exceed 0.01 % of the total REE concentration
M_r	the number of the spatial steps	fixed to 100

(f = 0.5) (e.g., Kretz, 1973, 1974). Which of the growth-rate laws is dominant depends on which of the kinetic processes is slower, the garnet growth rate or the diffusivity of the constituent material for the garnet. Especially, the diffusion-controlled growth is characterized by the presence of the diffusion halo of the major elements around the growing garnet porphyroblast. In contrast, a garnet porphyroblast which grew with the interface-controlled process ideally never should be accompanied by such diffusion halos. In the latter case, constituent materials for the garnet are homogeneously distributed in the matrix. Skora et al. (2006) estimated the growth-rate limiting process of their sample to be the interface-controlled by comparing major-element profiles of multiple garnets with different sizes; they assumed that the garnet growth kinetics is affected only by content of the major elements or the divalent cations, and that the major elements had been

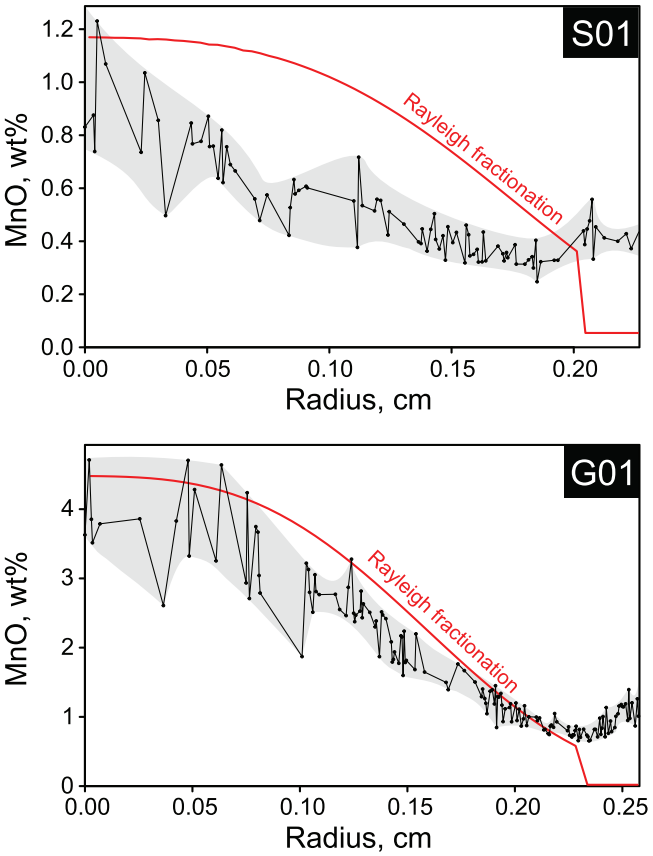

FIGURE 5 MnO profiles of the S01 (upper) and the G01 (lower) garnets. The gray bands roughly indicate their possible value ranges. Theoretical profiles based on the Rayleigh fractionation are also shown

in equilibrium over the matrix during the garnet growth based on the major-element compositional similarity among the garnets. However, due to the lack of enough samples, we cannot utilize the same method.

Alternatively, we judge the growth-rate limiting processes of our samples based only upon their own profiles, particularly focusing on the Mn profiles. If the bulk composition is homogeneous over the eclogite sample, the Mn profile in the garnet should be approximated by the bell-shaped profile caused by the Rayleigh fractionation (Hollister, 1966). Therefore, by evaluating the Mn profiles whether they are bell-shaped or not, we can estimate the growth-rate limiting processes in our samples. Figure 5 shows the MnO profiles in our samples and possible profiles with the Rayleigh fractionation. Excluding the outside portions of the Mn discontinuities, the S01 profile (MnO) cannot be reproduced by the bell-shaped profiles, while the G01 profile (MnO) can be approximated by the bell-shaped profile. Hence, we conclude that S01 'relatively' underwent the diffusion-controlled growth and that G01 underwent the interface-controlled growth. Nevertheless, it is still uncertain whether S01 grew with completely diffusion-controlled processes; the garnet sample of Skora et al. (2006) was estimated to have grown with the interface-controlled processes even though its Mn profile was not bell-shaped.

Here it should be noted that 'diffusion-controlled growth' and 'diffusion-limited REE uptake' are completely different ideas. Skora et al. (2006) assume that REE concentrations in garnet are too low to affect the growth kinetics and that only the major, divalent cation concentrations are the crucial factors. In this study, we adopt the idea and discuss the garnet-growth/REE-uptake rate laws. Judging from the Y + HREE profiles (Figures 3 and 4), no bell-shaped profiles are observed and many of them are characterized by the acute central peaks. Therefore, we assume that both of the investigated garnets underwent the diffusion-limited REE uptake. Importantly, considering that the Eu and Gd profiles in S01 have the extremely acute central peaks, a rate-law approximation that S01 'absolutely' grew with the diffusion-controlled processes can be reasonable. This is because a garnet which grew with the diffusion-controlled process generally has relatively prominent REE spikes at its core (Skora et al., 2006).

6.3 | Parameter optimization

Based on the measured REE profiles and estimated garnet-growth/REE uptake rate laws, we try to reproduce the feasible theoretical profiles with Skora et al.'s model to estimate some of the kinetic parameters. However, unfortunately, the most striking problem is that we consequently obtain almost the same REE profile even if we choose different parameter sets. In other words, succeeding in reproducing the real REE profile with the model does not necessarily mean the genuine parameter determination. For example, the Y profile in Skora et al.'s simulation can be reproduced with the other (D_0, α) values than those in their paper (e.g., $D_0 = 4.0 \times 10^{14}$ cm^2·yr^{-1}, $\alpha = 2.25 \times 10^{-7}$ cm·yr^{-1}). Thus, to evaluate the kinetic parameters properly, we have to elucidate the effect of the parameter fluctuation on the subsequently calculated profiles.

Drawing inspiration from the idea of 'the growth Péclet number' (e.g., Albarede & Bottinga, 1972; Hickmott & Shimizu, 1990; Watson, 1996; Watson & Müller, 2009), we attribute this parameter ambiguity problem to the definition of the parameters. The growth Péclet number is a dimensionless number for describing the trace-element uptake in a growing crystal. When the crystal radius is a linear function of time, we can define the number as $V{\cdot}L/D$, where V is the velocity at which the interface moves, L is the appropriate diffusive length scale (the width of the diffusive boundary layer), and D is the diffusion coefficient. Although the L value is hard to constrain unless we can measure distinct trace-element depletion in the natural eclogitic matrices, we can discuss it, at least based on a width variation of the diffusion halo simulated by Watson and Müller (2009). In a finite-sized spherical system whose radius is larger than the final garnet radius by ~1 mm, significant disequilibrium uptake in the garnet ($V/D \geq 1$ cm^{-1}) would lead to thin diffusion halos (typically ~10^{-1} mm order of magnitude), regardless of the V/D ratios. Thus, in our model situation, the V/D ratio is of critical importance for characterizing a

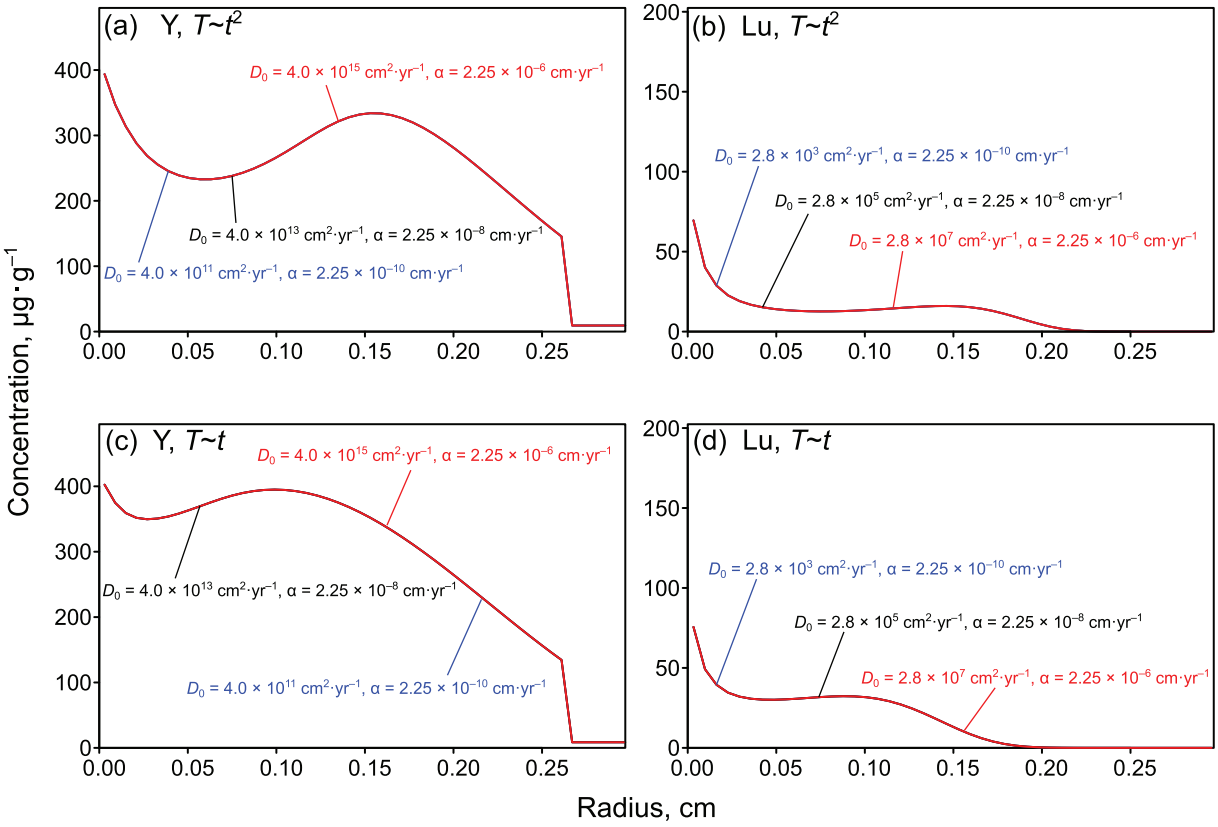

FIGURE 6 Simulation results for multiple D_0 and α values. The trace-element profiles in Skora et al. (2006) are reproduced with multiple sets of the (D_0, α) values whose ratios are constant: (a) Y, $T \sim t^2$; (b) Lu, $T \sim t^2$; (c) Y, $T \sim t$; (d) Lu, $T \sim t$

trace-element profile in a given garnet porphyroblast, at least practically. We therefore expect that, when f = 1, the ratio of the garnet growth rate to the diffusion coefficient can be the new, independent parameter. In other words, we assume that Skora et al.'s model generates the same REE profile with the different previous parameter sets only if the new parameter sets recalculated from them are the same. Since we cannot confirm this hypothesis explicitly, we test various parameter sets which meet this relationship whether they really generate the same REE profile.

Especially in our case, we define the new parameter as the reciprocal, or D/V, which refers to the diffusion coefficient normalized to the constant garnet growth rate. This definition is natural to consider core-to-rim profiles of various elements in a certain garnet porphyroblast. The new parameter D^* ($\equiv D/\alpha$) is expressed as:

$$D^* = \frac{D_0 \exp\left(-\frac{Q}{RT_{(t)}}\right)}{\alpha}. \quad (3)$$

This fractional number D^* contains the following variables: D_0, Q, α, and the function form of $T(t)$. Note that D^* is no longer a time-independent, constant parameter because it encompasses the function of time. As we mentioned, we expect that Skora et al.'s model generates the same REE profile with the same value of D^* if values of the other parameters than D^* are also the same. We test this hypothesis by: (Case 1) setting various D_0 and α values and fixing the other parameters; and (Case 2) setting various D_0 and Q values and fixing the other parameters. In each of the cases, we also check how the function form of temperature affects the simulation results.

Figures 6 and 7 show the simulation results for Cases 1 and 2, respectively. As we set various D_0 and α values fixing the other parameters (Case 1), we found that we obtained, at least macroscopically, the identical REE profile when their ratio was fixed. Figure 6a,b shows that the Lu and Y profiles in Skora et al.'s simulation can be reproduced by setting various assemblages of D_0 and α, fixing their ratio to 1.78×10^{21} and 1.24×10^{13} cm, respectively. Moreover, this phenomenon is observed even when the function form of temperature is changed from $T \sim t^2$, which is adopted in the case of Skora et al. (2006). Figure 6c,d describes this phenomenon, especially when we adopt $T \sim t$, fixing the other parameters to the same as the case of Figure 6a,b. Considering that these conditions for the REE profiles are not likely to be the particular solutions, it is natural that the effects of D_0 and α compensate for each other, and that this relationship is valid for any function forms of temperature. This independence of the simulation results from the function forms of temperature is probably because D^* would be kept constant at each of the time steps even if we adopt any forms of functions as temperature.

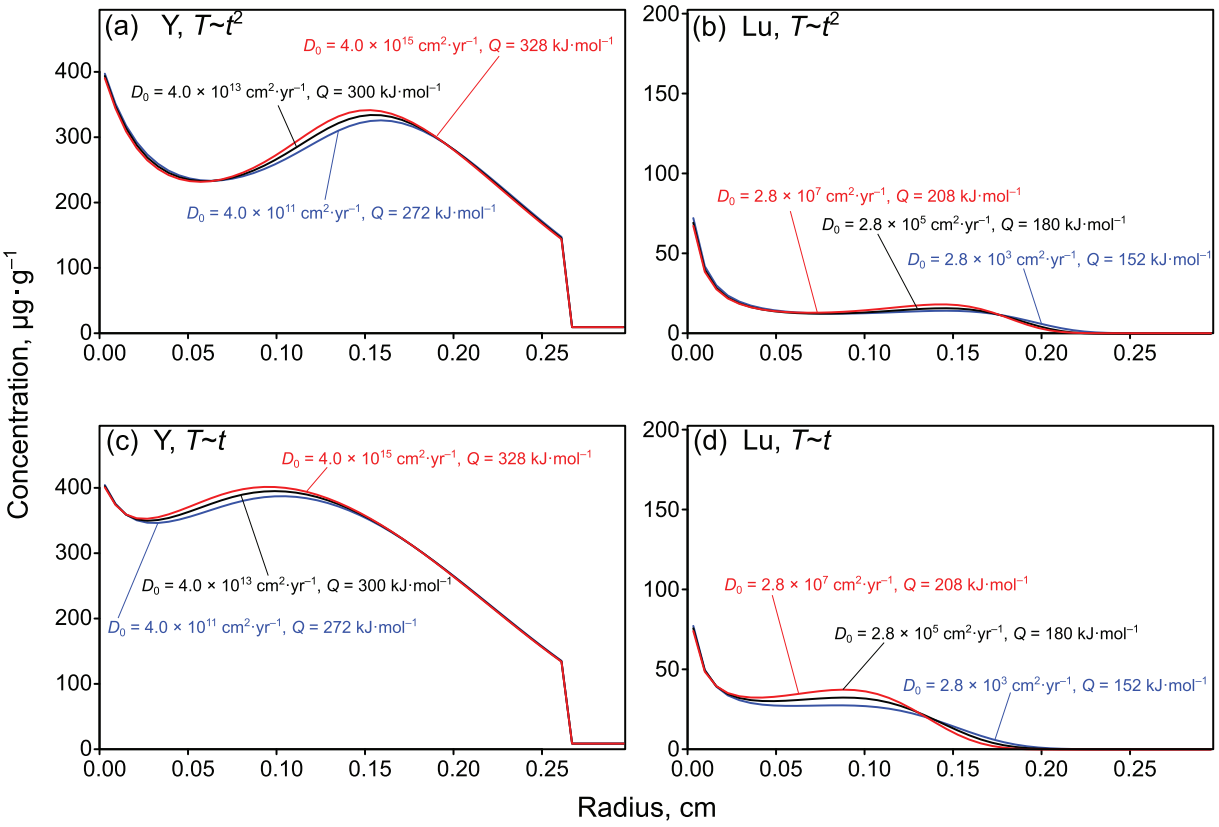

FIGURE 7 Simulation results for multiple D_0 and Q values. The trace-element profiles in Skora et al. (2006) are reproduced with multiple sets of the (log D_0, Q) values which have linear relationships: (a) Y, $T \sim t^2$; (b) Lu, $T \sim t^2$; (c) Y, $T \sim t$; (d) Lu, $T \sim t$. All the α values are fixed to 2.25×10^{-8} cm·yr^{-1}

On the other hand, Figure 7a–d shows the similar cases as setting various D_0 and Q values and fixing the other parameters (Case 2). Figure 7a,b is the result when $T \sim t^2$, while Figure 7c,d is that when $T \sim t$. We found that, if we fixed the values of log D_0 and Q so that they could satisfy linear relationships, we obtained approximately the same REE profiles. Although they are not completely the same, we can ignore their difference as smaller one than the measurement errors. This linear relationship between log D_0 and Q can be explained as follows. When we fix both of D^* and α to constant values, the logarithm of their product is expressed as:

$$\log D^* \alpha = \log D_0 + \frac{1}{\ln 10}\left(-\frac{Q}{RT_{(t)}}\right). \quad (4)$$

Rearranging, we get

$$\log D_0 = \log D^* \alpha + \frac{Q}{2.303RT_{(t)}}. \quad (5)$$

This means that, if the initial/final temperature difference is small enough, log D_0 should be approximated by a linear function of Q in order to fix D^* and α to constant values. Since we adopt 450–600 °C, the typical temperature range of the low-T eclogite, as the temperature range in all of the examples above, if it is small enough for the presence of the pseudo-linear relationship between log D_0 and Q, we can expect this relationship to be common among any low-T eclogite. Comprehensively, we conclude that the ratio of the diffusion coefficient to the garnet growth rate can be the new, independent parameter (D^*) when $f = 1$.

6.4 | Procedure of the parameter determination

As we succeeded in defining the new parameter D^* and solving the parameter ambiguity problem, we describe the procedure of the parameter determination with our REE-uptake model. Firstly, we show what kind of parameter values we can set prior to the REE-profile calculation. Since the model includes a number of parameters, in order to adjust theoretical REE profiles to the real REE profile efficiently, we have to fix some parameters whose values are already known or can be approximated. In this study, we fix the following parameters for each of the trace-elements in each of the garnets: (1) C_{ave}, (2) R_{gar}, (3) K, (4) T_1 and T_2, and (5) f_T (the function form of temperature). Note that the exponent of the garnet-growth law (f) is fixed to 1. We simply adopt the measured bulk-rock concentration of the trace-element and the real size of the garnet as C_{ave} and R_{gar}, respectively. Then, since K and C_{ave} are the only parameters which determine the core concentration of the theoretical profile, we can approximately fix the K value for a given natural REE profile. Unfortunately, the T–t path is the least constrained parameter. Nevertheless, we adopt the metamorphic peak temperature obtained from the literature as T_2, and we assume $T \sim t^2$ paths for the model calculation. The latter assumption is based on the idea that heating of a slab is more rapid once exhumation (e.g., Roselle & Engi, 2002), as with Skora et al. (2006). At last, we choose the appropriate T_1 values on the assumption that almandine garnets in the low-T eclogite never nucleate at temperatures lower than 450 °C (e.g., Massonne & Li, 2020). We are obliged to adopt this approximation because we cannot estimate the T_1 value even if we utilize the garnet–clinopyroxene geothermometry (Ravna, 2000) due to the thermal overstepping of the garnet nucleation (e.g., Gaidies et al., 2011).

We afterwards set multiple values of the genuine 'variable parameters', which are the remaining ones: u, Q, and R_{sys}, to find out the appropriate theoretical REE profile. Note that the new parameter u, which is the ratio of D_0 and α, is introduced here. This formulation leads to the simplest expression of D^*, i.e., $D^* = u \cdot \exp(-Q/RT_{(t)})$. Actually, D^* is not viable for applying the model directly to natural samples because of its time-dependency. Specifically, as running our computer program for the REE-uptake 'forward' modeling, we can set certain values only for time-independent parameters. Thus, for practical and systematic use of this uptake model with the new-defined parameter D^*, we have defined this new time-independent parameter here. By introducing u, we can rewrite Equation (5) as:

$$\log u = \log D^* + \frac{Q}{2.303RT_{(t)}}. \quad (6)$$

On the basis of the discussion above (see Section 6.3), a REE profile of a low-T eclogite garnet, which is mainly characterized by a certain D^* value, should ideally be expressed with certain values of the parameters including multiple sets of the pseudo-linearly related parameters: log u and Q. Since both encompass information on the kinetics of garnet growths and/or REE diffusion, plotting all of the possible (u, Q) values and comparing them among different natural garnets graphically would be valuable for the elucidating the kinetics of the low-T eclogitization. In other words, we have no choice but to identify how the multiple possible (u, Q) values are correlated to each other to keep the D^* value nearly constant.

We found that u and Q fluctuations similarly affected the REE profiles around their secondary peaks, and that R_{sys} affect only their rims (Figure 8a). In this case, the effective contributions of the u–Q fluctuations and the R_{sys} fluctuation to the REE-profile shapes are almost independent from each other. Thus, we can adjust calculated REE profiles to the natural profile only by choosing the reasonable, pseudo-linearly related (log u, Q) value assemblages and the reasonable R_{sys} value, so that the steepness of the central peak and the rim concentration of the natural profile can be reproduced by the theoretical one. Rigorously, since the remaining REE content in the matrix at a given time obviously depends upon the garnet REE content at that time, the effective contributions of the u–Q and the R_{sys} fluctuation to the REE-profile shapes are not independent. However, this interaction is quite small because the volume of the inner sphere shell is smaller than that of the outer shell, and because the fluctuation of the REE-profile shapes affected by u and Q has no significant effect on the remaining matrix REE content.

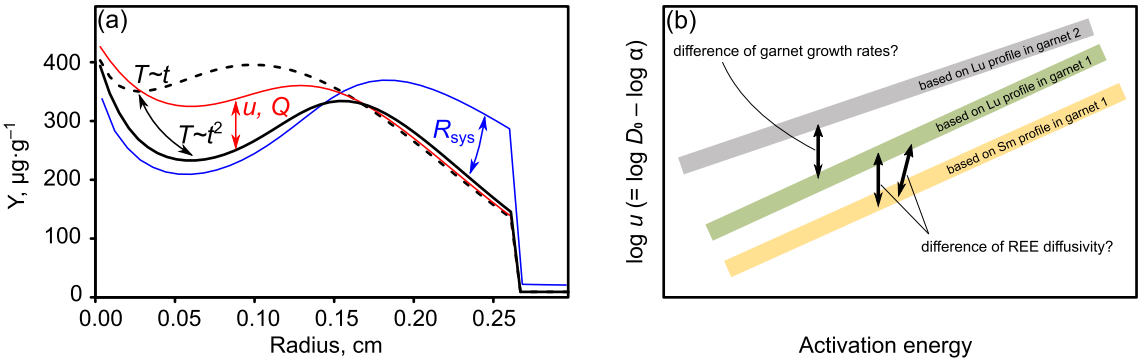

FIGURE 8 Schematic diagrams which explain our new model-interpretation: (a) effects of parameter fluctuation on the Y profile of Skora et al. (2006). The black solid line is calculated with the same parameter set as theirs, and the red, blue and dotted lines are calculated with $u = 5 \times 10^{21}$ cm, $R_{sys} = 0.80$ cm and $T \sim t$, respectively. In each of the cases, the other parameters are the same as that of the black solid line. The shape of the T–t curve, u and Q affect the REE profile relatively near the core of the garnet, while R_{sys} affects near the rim; (b) schematic log u–Q correlation diagram. Based on the different REE profiles in the same garnet (green and yellow lines), we would be able to compare their diffusivities, while the profiles of the same trace-element in different garnets which share the same eclogitic matrix (gray and green lines) would unravel the difference between their growth rates

6.5 | Visualization of the newly defined parameter

Up to this point, we have individually determined the reasonable parameter values except for u and Q, and have found a correlation among the multiple possible (u, Q) sets. This log u–Q relationship, which highly reflects the common, almost fixed D^* value, can be approximated by a linear function. When Equation (6) shows the pseudo-linear correlation between log u and Q values, we can tentatively rewrite it for interpreting the obtained parameter values as:

$$\log u = \log D^*_{\mathrm{eff}} + \frac{Q}{2.303RT_{\mathrm{eff}}}, \tag{7}$$

where D^*_{eff} and T_{eff} mean fictional, time-independent values for D^* and temperature, respectively. However, it would actually be difficult to precisely determine these fictional values due to the large analytical errors, and subsequent uncertainty about the estimated intercept/gradient values for the correlated line. Specifically, even if we can obtain a certain correlated line between the log u and Q values, it must be like a thick 'band' rather than a sharp line. Actually, although we can calculate a D^*_{eff} value from a certain (u, Q) pair with an arbitrary T_{eff} value, this means we cannot consider the real temperature path, which is highly important for explaining secondary peaks of M-shaped profiles. Nevertheless, as we can draw this 'band' on a log u–Q graph for the each REE and for multiple garnets, the significant intercept/gradient difference among the obtained bands are, if presented, of potential application for comparing the REE-diffusion/garnet-growth kinetics in the different settings.

Since the temperature ranges for the low-T eclogite are not much different, it would be useful to compare the intercepts of the correlation lines (bands) to discuss the difference of the D^*_{eff} values. When either the REE diffusivity or the garnet growth rate is already known, this comparison highly constrains the other, unknown kinetic information, because the D^* (D^*_{eff}) value represents the ratio of the diffusivity to the garnet growth rate (Figure 8b). For example, by applying this method to a garnet whose growth duration is already known with the radiometric isotope analyses, we would be able to clarify the difference of the diffusivity in the host eclogite. Inversely, by applying this to multiple garnets which share the same eclogitic matrix, we should be able to determine the difference of their growth rates and might be able to discuss the heterogeneous spatial distribution of the growth rates. In any case, our new formulation of the REE-uptake model allows us to estimate such valuable parameters based on the real REE profiles with a one-to-one correspondence, and leads to the simple quantitative characterization of core-to-rim REE profiles in a porphyroblastic garnet in low-T eclogite.

6.6 | Model application (parameter determination)

We established the new way of the model interpretation for garnets which grow with the interface-controlled processes. Here, we provide the proper values of the newly defined parameters for the sample G01. This sample is appropriate for the analysis because its REE profiles contain the signals from the genuine garnet core, and because the garnet would have grown with the interfaced-controlled process. Since the Sm, Eu, Gd profiles have highly scattered values at the rim, we apply the model only to the other Y + HREE profiles.

Firstly, we set the prerequisite values to the analysis, C_{ave}, R_{gar}, and its temperature path. The C_{ave} values are taken from the bulk-rock composition of the Type-II lawsonite eclogite of the SMM presented in Hara et al. (2018). We approximate the REE compositions of our sample the same as this, although their different rock types, probably due to the extent of the retrograde metamorphism (Tsujimori et al., 2006b), would make a slight difference in their bulk REE compositions. The R_{gar} value is set as 0.2345 cm, excluding the overgrowth rim. The initial/final temperatures are respectively fixed to 450 and

480 °C based on the estimation of the prograde stage by Tsujimori et al. (2006b).

Then, for each of the profiles, we adjust u values so that the measured data can be successfully reproduced by the theoretical profiles by fixing the Q values. For example, Figure 9a shows the result for the Y profile with Q = 300 kJ·mol^{-1}. In this case, we obtained the log u values of 21.3–22.2 with R_{sys} = 0.40 cm and with K = 75. The results for all of the elements with Q = 300 kJ ·mol^{-1} are presented in Figure 9b, which suggests all of the u values are ~10^{21-22} cm though

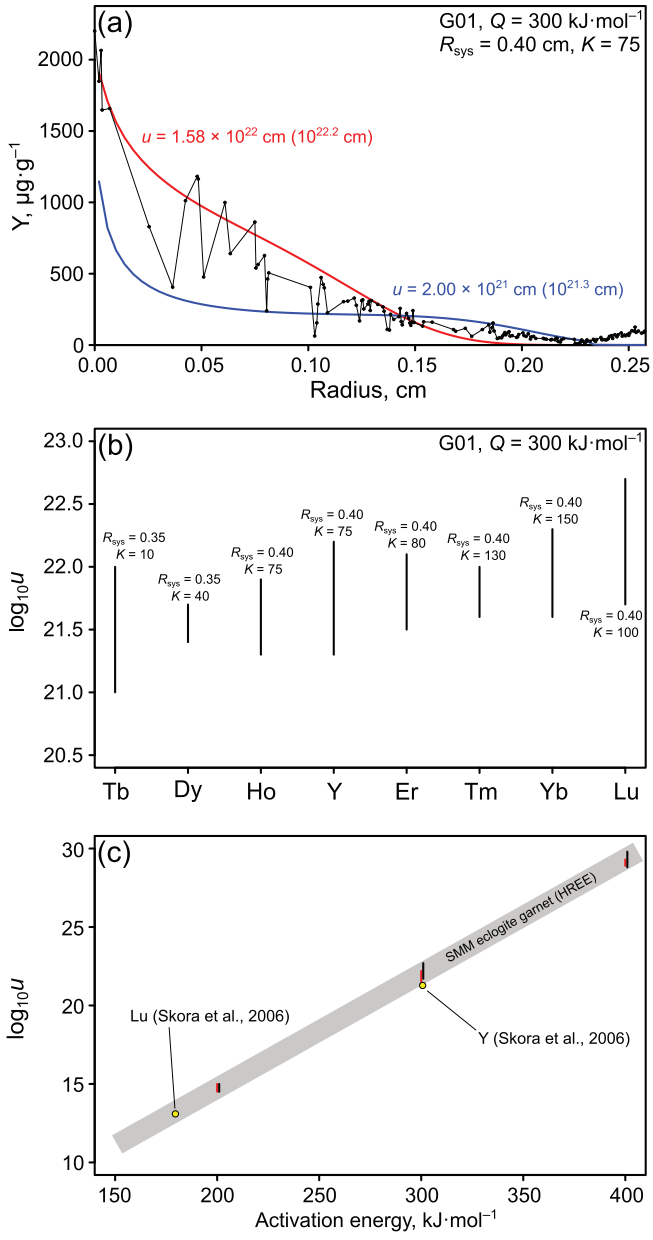

FIGURE 9 Results of the parameter determination for the garnet G01: (a) analysis of the Y profile with Q = 300 kJ·mol^{-1}; (b) summary of the results with Q = 300 kJ ·mol^{-1}; (c) the approximate correlation line for the Y + HREE profiles in the garnet G01 (the gray band). The red and black bars indicate the representative u values of the Y and Lu profiles in G01, respectively. The yellow circles indicate the reference values from Skora et al. (2006)

the elements with larger atomic numbers tend to yield larger u values. Since the estimation error for u values for a certain element amounts to ~1 order of magnitude, it turns out to be difficult to clarify the difference of diffusivities among Y + HREEs. Our analysis also shows that the K value tends to increase according as the atomic number increases, and that the R_{sys} values are smaller for Tb and Dy than for the other elements. Although it is somewhat strange that R_{sys} values for different elements are not equal, this unfavorable consequence is inevitable with our parameter-determination procedure. This is because, in our case, the R_{sys} values depend upon the measured concentration at the garnet rim and the whole-rock concentration of the element. This point is different from the idea of Skora et al. (2006) in that they estimated the R_{sys} value from the distance between nearest garnet porphyroblasts. We can attribute this contradiction to (1) the difference between the real and the literature concentration; or (2) external infiltration of more diffusive elements. Hence, the obtained trends in the K and R_{sys} values are consistent with the physicochemical properties of HREEs. Specifically, their smaller ionic radii would lead to their larger diffusion coefficients (e.g., Cherniak et al., 1997; Tirone et al., 2005; Van Orman et al., 2001), and would let themselves be more highly incorporated into garnet (e.g., Sassi et al., 2000).

Finally, by setting other Q values, we obtained the correlation line in a log u–Q graph (Figure 9c). Although we succeeded in simply visualizing the relationship between the garnet-growth rate and the REE diffusivity in the lawsonite eclogite in the SMM, we cannot see any distinctive intercept-differences between the results for the different elements. Nevertheless, intriguingly, we found that the (u, Q) values calculated from the simulation results of Skora et al. (2006) were consistent with our correlation band. For example, Skora et al.'s u value just corresponds to the lowest value of the SMM eclogite for the Y profiles. This means that the u–Q correlation lines of the SMM lawsonite eclogite (our sample) and the Zermatt-Saas Fee eclogite (Skora et al.'s sample) are almost identical.

6.7 | Implications for the garnet-growth/REE-diffusion kinetics

The most crucial results in our study are: (i) the SMM garnet grew with the interface-controlled processes, while the Syros garnet probably underwent the diffusion-controlled processes; (ii) both underwent the diffusion-limited REE uptake; and (iii) the u–Q relationship for the SMM eclogite is similar to that of the Zermatt-Saas Fee eclogite. Considering the result of (iii), if the cation diffusivity in the SMM eclogite is the same as that of the Zermatt-Saas Fee eclogite, one can conclude that the growth rate in the SMM eclogite is same as (or an order of magnitude smaller than) that in the Zermatt-Saas Fee eclogite. However, due to lack of information on the diffusion kinetics in the individual rocks, we cannot confirm whether this statement is correct only with the model analyses.

Thus, let us discuss the garnet-growth/REE-diffusion kinetics by considering also other factors than the REE-uptake model.

Specifically, some previous geochronological analyses of garnets have elucidated their growth durations. Lagos et al. (2007) showed that some Lu–Hf ages of differently Lu-zoned garnets from low-*T* eclogite in Syros were almost the same within error. The age deviation was only ~1.4 Ma, which indicates that a timescale of garnet growth in Syros eclogite is significantly small, perhaps only a few million years. On the other hand, Brueckner et al. (2009) showed highly scattered Sm–Nd ages of garnets from the SMM eclogites and estimated the span of the garnet growth was up to ~20 Myr. This suggests that the Syros garnet grew an order of magnitude faster than the SMM garnet. In addition, as a first-order assumption, the growth span of the Syros garnet is longer than that of the Zermatt-Saas Fee garnet. It is because the major mineral assemblages of the Zermatt-Saas Fee eclogite are not much different from those of the Syros eclogite (Skora et al., 2006), which indicates the both garnet-forming reactions would be similar, and because, in order to explain the result of (i), the cation diffusivity in the Syros eclogite should be lower than the Zermatt-Saas Fee eclogite. Hence, we can estimate that the Zermatt-Saas Fee garnet grew a few orders of magnitude faster than the SMM garnet, and subsequently conclude that their cation diffusivities are different. In summary, we can envisage that the cation diffusivities in low-*T* eclogites would generally be diverse. This is probably attributed to the difference in chemical composition of fluids and water/oxygen fugacities, because cation diffusion in minerals or their aggregates generally depends on such factors (e.g., Carlson, 2002; Farver & Yund, 2000; Hiraga et al., 2004; Van Orman et al., 2001).

For deeper understanding of the garnet-growth/REE-diffusion kinetics, we additionally estimate 'approximated' D^*_{eff} values for the Y + HREE profiles in G01. Choosing the Y profile with Q = 300 kJ·mol^{-1} as the representative one, the calculated D^*_{eff} values are: ~0.4–3 cm (450 °C); and~3–20 cm (480 °C). The reciprocal values of the obtained D^*_{eff} values would correspond to the V/D values: 0.3–3 cm^{-1} (450 °C); and 0.05–0.3 cm^{-1} (480 °C). Assuming that the reasonable V/D values for disequilibrium uptake range from ~1 to ~100 cm^{-1} at most (Watson & Müller, 2009), the extent of disequilibrium Y uptake into G01 is relatively small. Thus, it is natural that the G01 growth rate should be lower than other garnets from different localities. On the other hand, considering their assumption that the possible range of V/D values is small (~2 orders of magnitude), we perhaps cannot obtain any valuable kinetic information depending on a degree of uncertainty about the D^*_{eff} determination, mainly due to the large analytical errors.

Here we have shown that garnets in the low-*T* eclogite have a potential to provide more information on the chemical geodynamics in subduction zones than expected before. Our simple quantitative characterization of the core-to-rim REE profiles would particularly facilitate discussion of the cation diffusion kinetics in natural rocks, which are generally difficult to analyze due to the complicated diffusion processes there. Although we failed to evaluate the difference in garnet-forming reaction rates between the Syros and the SMM eclogites based only on the REE-uptake model analyses, our innovative way of interpreting REE-profiles in garnets would lead to a deeper understanding of the cation diffusion kinetics in subduction zones.

7 | CONCLUSION

We measured the major/trace element profiles of the low-*T* eclogite garnets obtained from Syros (Greece) and the SMM (Guatemala). Comparing the measured data to the theoretical profiles generated with the diffusion-limited REE-uptake model, we determined their growth kinetics (Syros: diffusion-controlled; SMM: interface-controlled) and REE-uptake kinetics (both: diffusion-limited). In addition, for garnets which grow with the interface-controlled processes, we reformulated the parameters of the REE-uptake model to elucidate their growth kinetics and the REE diffusivity and evaluated them for the SMM eclogite. Specifically, we proposed that the ratio of a certain REE diffusion coefficient nearby the garnet to its growth rate could be regarded as the new parameter to characterize REE profiles in the garnets. We expect this to contribute to the estimation of the garnet-growth/REE-diffusion kinetics with a one-to-one correspondence. We concluded that our new model interpretation would give clues to unraveling the cation-diffusion processes in low-*T* eclogite, subsequently the comprehensive understanding of the chemical geodynamics in subduction zones.

ACKNOWLEDGMENTS

This research was supported by CNEAS at Tohoku University in part by grants from the MEXT/JSPS KAKENHI JP15H05212 and JP18H01299 to Tatsuki Tsujimori. This was also supported by MEXT Private University Research Branding Project (Okayama University of Science) to Kazumasa Aoki and JSPS KAKENHI JP19K04043 to Kazumasa Aoki. Tatsuki Tsujimori and Ryo Fukushima acknowledge the International Joint Graduate Program in Earth and Environmental Sciences (GP-EES) and the JSPS Japanese–German Graduate Externship. The authors thank Daniel Pastor-Galán for his feedback. We are deeply grateful to Tadao Nishiyama and the anonymous reviewer for the highly stimulating discussion, and Yuji Ichiyama for his editorial handling of this manuscript.

ORCID

Ryo Fukushima https://orcid.org/0000-0003-2683-6757
Tatsuki Tsujimori https://orcid.org/0000-0001-9202-7312
Shogo Aoki https://orcid.org/0000-0001-5093-1346
Kazumasa Aoki https://orcid.org/0000-0001-7645-6766

REFERENCES

Albarede, F., & Bottinga, Y. (1972). Kinetic disequilibrium in trace element partitioning between phenocrysts and host lava. *Geochimica et Cosmochimica Acta*, *36*, 141–156.

Banno, S., & Chii, S. (1978). A model to explain the Mn enrichment in the rim of zoned garnet. *Geochemical Journal*, *12*, 253–257.

Baxter, E. F., Caddick, M. J., & Ague, J. J. (2017). Garnet: Common mineral, uncommonly useful. *Elements*, *9*, 415–419.

Baxter, E. F., Caddick, M. J., & Dragovic, B. (2013). Garnet: A rock-forming mineral petrochronometer. *Reviews in Mineralogy and Geochemistry*, *83*, 469–533.

Brueckner, H. K., Avé Lallemant, H. G., Sisson, V. B., Harlow, G. E., Hemming, S. R., Martens, U., Tsujimori, T., & Sorensen, S. S. (2009). Metamorphic reworking of a high pressure-low temperature mélange along the Motagua fault, Guatemala: A record of Neocomian and Maastrichtian transpressional tectonics. *Earth and Planetary Science Letters*, *284*, 228–235.

Caddick, M. J., Konopásek, J., & Thompson, A. B. (2010). Preservation of garnet growth zoning and the duration of prograde metamorphism. *Journal of Petrology*, *51*, 2327–2347.

Carlson, W. D. (2002). Scales of disequilibrium and rates of equilibration during metamorphism. *American Mineralogist*, *87*, 185–204.

Carlson, W. D. (2012). Rates and mechanism of Y, REE, and Cr diffusion in garnet. *American Mineralogist*, *97*, 1598–1618.

Cherniak, D. J., Hanchar, J. M., & Watson, E. B. (1997). Rare-earth diffusion in zircon. *Chemical Geology*, *134*, 289–301.

Christensen, J. N., Rosenfeld, J. L., & DePaolo, D. J. (1989). Rates of tectonometamorphic processes from rubidium and strontium isotopes in garnet. *Science*, *244*, 1465–1469.

Crank, J. (1975). *The mathematics of diffusion*. Oxford: Oxford University Press.

Enami, M., Nishiyama, T., & Mouri, T. (2007). Laser Raman microspectrometry of metamorphic quartz: A simple method for comparison of metamorphic pressures. *American Mineralogist*, *92*, 1303–1315.

Farver, J. R., & Yund, R. A. (2000). Silicon diffusion in forsterite aggregates: Implications for diffusion accommodated creep. *Geophysical Research Letters*, *27*, 2337–2340.

Fukushima, R., Tsujimori, T., & Miyajima, N. (in press). Various antiphase domains in garnet-hosted omphacite in low temperature eclogite: A FIB–TEM study on heterogeneous ordering processes. *American Mineralogist*. https://doi.org/10.2138/am-2021-7784

Fukuyama, M., Ogasawara, M., Sato, H., & Ishiyama, D. (2007). Trace element analysis of gem garnet by LA-ICP-MS: Preliminary evaluation as micro-beam standard. *Bulletin of the Geological Survey of Japan*, *58*, 93–103 (in Japanese with English abstract).

Gaidies, F., Pattison, D. R. M., & de Capitani, C. (2011). Toward a quantitative model of metamorphic nucleation and growth. *Contributions to Mineralogy and Petrology*, *162*, 975–993.

Hara, T., Tsujimori, T., Chang, Q., & Kimura, J. -I. (2018). *In-situ* Sr–Pb isotope geochemistry of lawsonite: A new method to investigate slab-fluids. *Lithos*, *320–321*, 93–104.

Harlow, G. E., Hemming, S. R., Avé Lallemant, H. G., Sisson, V. B., & Sorensen, S. S. (2004). Two high-pressure–low-temperature serpentinite-matrix mélange belts, Motagua fault zone, Guatemala: A record of Aptian and Maastrichtian collisions. *Geology*, *32*, 17–20.

Hesse, M. A. (2012). A finite volume method for trace element diffusion and partitioning during crystal growth. *Computers & Geosciences*, *46*, 96–106.

Hickmott, D. D., & Shimizu, N. (1990). Trace element zoning in garnet from the Kwoiek area, British Columbia: Disequilibrium partitioning during garnet growth? *Contributions to Mineralogy and Petrology*, *104*, 619–630.

Hiraga, T., Anderson, I. M., & Kohlstedt, D. L. (2004). Grain boundaries as reservoirs of incompatible elements in the Earth's mantle. *Nature*, *427*, 699–703.

Hollister, L. S. (1966). Garnet zoning: An interpretation based on the Rayleigh fractionation model. *Science*, *154*, 1647–1651.

Inui, M., & Toriumi, M. (2004). A theoretical study on the formation of growth zoning in garnet consuming chlorite. *Journal of Petrology*, *45*, 1369–1392.

Kim, H. S. (2006). Deformation-induced garnet zoning. *Gondwana Research*, *10*, 379–388.

Kohn, M. J. (2009). Models of garnet differential geochronology. *Geochimica et Cosmochimica Acta*, *73*, 170–182.

Kohn, M. J., Valley, J. W., Elsenheimer, D., & Spicuzza, M. J. (1993). O isotope zoning in garnet and staurolite: Evidence for closed-system mineral growth during regional metamorphism. *American Mineralogist*, *78*, 988–1001.

Konrad-Schmolke, M., Handy, M. R., Babist, J., & O'Brien, P. J. (2005). Thermodynamic modelling of diffusion-controlled garnet growth. *Contributions to Mineralogy and Petrology*, *149*, 181–195.

Kretz, R. (1973). Kinetics of the crystallization of garnet at two localities near yellowknife. *The Canadian Mineralogist*, *12*, 1–20.

Kretz, R. (1974). Some models for the rate of crystallization of garnet in metamorphic rocks. *Lithos*, *7*, 123–131.

Lagos, M., Scherer, E. E., Tomaschek, F., Münker, C., Keiter, M., Berndt, J., & Ballhaus, C. (2007). High precision Lu–Hf geochronology of Eocene eclogite-facies rocks from Syros, Cyclades, Greece. *Chemical Geology*, *243*, 16–35.

Lapen, T. J., Johnson, C. M., Baumgartner, L. P., Mahlen, N. J., Beard, B. L., & Amato, J. M. (2003). Burial rates during prograde metamorphism of an ultra-high-pressure terrane: An example from Nago de Cignana, western Alps, Italy. *Earth and Planetary Science Letters*, *215*, 57–72.

Laurent, V., Jolivet, L., Roche, V., Augur, R., Scarlet, S., & Cardello, G. L. (2016). Strain localization in a fossilized subduction channel: Insights from the Cycladic Blueschist Unit (Syros, Greece). *Tectonophysics*, *672*, 150–169.

Laurent, V., Lanari, P., Naïr, I., Augier, R., Lahfid, A., & Jolivet, L. (2018). Exhumation of eclogite and blueschist (Cyclades, Greece): Pressure–temperature evolution determined by thermobarometry and garnet equilibrium modeling. *Journal of Metamorphic Geology*, *36*, 769–798.

Lister, G. S., & Forster, M. A. (2016). White mica $^{40}Ar/^{39}Ar$ age spectra and the timing of multiple episodes of high-P metamorphic mineral growth in the Cycladic eclogite–blueschist belt, Syros, Aegean Sea, Greece. *Journal of Metamorphic Geology*, *34*, 401–421.

Massonne, H. -J., & Li, B. (2020). Zoning of eclogitic garnet cores – A key pattern demonstrating the dominance of tectonic erosion as part of the burial process of worldwide occurring eclogites. *Earth-Science Reviews*, *210*, 103356.

Moore, S. J., Carlson, W. D., & Hesse, M. A. (2013). Origins of yttrium and rare earth element distributions in metamorphic garnet. *Journal of Metamorphic Geology*, *31*, 663–689.

Pearce, N. J. G., Perkins, W. T., Westgate, J. A., Gorton, M. P., Jackson, S. E., Neal, C. R., & Chenery, S. P. (1997). A compilation on new and published major and trace element data for NIST SRM 610 and NIST SRM 612 glass reference materials. *Geostandards Newsletter*, *21*, 115–144.

Pollington, A. D., & Baxter, E. F. (2010). High resolution Sm–Nd garnet geochronology reveals the uneven pace of tectonometamorphic processes. *Earth and Planetary Science Letters*, *293*, 63–71.

Raimondo, T., Payne, J., Wade, B., Lanari, P., Clark, C., & Hand, M. (2017). Trace element mapping by LA-ICP-MS: Assessing geochemical mobility in garnet. *Contributions to Mineralogy and Petrology*, *172*, 17.

Ravna, E. K. (2000). The garnet–clinopyroxene Fe^{2+}–Mg geothermometer: An updated calibration. *Journal of Metamorphic Geology*, *18*, 211–219.

Roselle, G. T., & Engi, M. (2002). Ultra high pressure (UHP) terrains: Lessons from thermal modeling. *American Journal of Science*, *302*, 410–441.

Sakai, C., Banno, S., Toriumi, M., & Higashino, T. (1985). Growth history of garnet in pelitic schists of the Sanbagawa metamorphic terrain in Central Shikoku. *Lithos*, *18*, 81–95.

Sassi, R., Harte, B., Carswell, D. A., & Yujing, H. (2000). Trace element distribution in Central Dabie eclogites. *Contributions to Mineralogy and Petrology*, *139*, 298–315.

Schumacher, J. C., Brady, J. B., Cheney, J. T., & Tonnsen, R. R. (2008). Glaucophane-bearing marbles on Syros, Greece. *Journal of Petrology*, *49*, 1667–1686.

Seck, H. A., Kötz, J., Okrusch, M., Seidel, E., & Stosch, H. -G. (1996). Geochemistry of a meta-ophiolite suite: An association of metagabbros, eclogites and glaucophanites on the island of Syros, Greece. *European Journal of Mineralogy*, *8*, 607–623.

Skora, S., Baumgartner, L. P., Mahlen, N. J., Johnson, C. M., Pilet, S., & Hellebrand, E. (2006). Diffusion-limited REE uptake by eclogite garnets and its consequences for Lu–Hf and Sm–Nd geochronology. *Contributions to Mineralogy and Petrology*, *152*, 703–720.

Spear, F. S., & Selverstone, J. (1983). Quantitative P–T paths from zoned minerals: Theory and tectonic applications. *Contributions to Mineralogy and Petrology*, *83*, 348–357.

Suzuki, T., Sakata, S., Makino, Y., Obayashi, H., Ohara, S., Hattori, K., & Hirata, T. (2018). iQuant2: Software for rapid and quantitative imaging using laser ablation-ICP mass spectrometry. *Mass Spectrometry*, *7*, A0065.

Tan, Z., Agard, P., Gao, J., Hong, T., & Wan, B. (2020). Concordant pulse in Mn, Y and HREEs concentrations during UHP eclogitic garnet growth: Transient rock dynamics along a cold subduction plate interface. *Earth and Planetary Science Letters*, *530*, 115908.

Tirone, M., Ganguly, J., Dohmen, R., Langenhorst, F., Hervig, R., & Becker, H. -W. (2005). Rare earth diffusion kinetics in garnet: Experimental studies and applications. *Geochimica et Cosmochimica Acta*, *69*, 2385–2398.

Tomaschek, F., Kennedy, A. K., Villa, I. M., Lagos, M., & Ballhaus, C. (2003). Zircons from Syros, Cyclades, Greece—Recrystallization and mobilization of zircon during high-pressure metamorphism. *Journal of Petrology*, *44*, 1977–2002.

Tribuzio, R., Messiga, B., Vannucci, R., & Botazzi, P. (1996). Rare earth element redistribution during high-pressure–low-temperature metamorphism in ophiolitic Fe-gabbros (Liguria, northwestern Italy): Implications for light REE mobility in subduction zones. *Geology*, *24*, 711–714.

Trotet, F., Vidal, O., & Jolivet, L. (2001). Exhumation of Syros and Sifnos metamorphic rocks (Cyclades, Greece). New constraints on the PT paths. *European Journal of Mineralogy*, *13*, 901–920.

Tsujimori, T., & Ernst, W. G. (2014). Lawsonite blueschists and lawsonite eclogites as proxies for palaeo-subduction zone processes: A review. *Journal of Metamorphic Geology*, *32*, 437–454.

Tsujimori, T., Liou, J. G., & Coleman, R. G. (2005). Coexisting retrograde jadeite and omphacite in a jadeite-bearing lawsonite eclogite from the Motagua Fault Zone, Guatemala. *American Mineralogist*, *90*, 836–842.

Tsujimori, T., Sisson, V. B., Liou, J. G., Harlow, G. E., & Sorensen, S. S. (2006a). Very-low-temperature record of the subduction process: A review of worldwide lawsonite eclogites. *Lithos*, *92*, 609–624.

Tsujimori, T., Sisson, V. B., Liou, J. G., Harlow, G. E., & Sorensen, S. S. (2006b). Petrologic characterization of Guatemalan lawsonite eclogite: Eclogitization of subjected oceanic crust in a cold subduction zone. *Geological Society of America Special Paper*, *403*, 147–168.

Uunk, B., Brouwer, F., ter Voorde, M., & Wijbrans, J. (2018). Understanding phengite argon closure using grain fusion age distribution in the Cycladic Blueschist Unit on Syros, Greece. *Earth and Planetary Science Letters*, *484*, 192–203.

Van Orman, J. A., Grove, T. L., & Shimizu, N. (2001). Rare earth element diffusion in diopside: Influence of temperature, pressure, and ionic radius, and an elastic model for diffusion in silicates. *Contributions to Mineralogy and Petrology*, *141*, 687–703.

Watson, E. B. (1996). Surface enrichment and trace-element uptake during crystal growth. *Geochimica et Cosmochimica Acta*, *24*, 5013–5020.

Watson, E. B., & Müller, T. (2009). Non-equilibrium isotopic and elemental fractionation during diffusion-controlled crystal growth under static and dynamic conditions. *Chemical Geology*, *267*, 111–124.

Yardley, B. W. D., Rochelle, C. A., Barnicoat, A. C., & Lloyd, G. E. (1991). Oscillatory zoning in metamorphic minerals: An indicator of infiltration metasomatism. *Mineralogical Magazine*, *55*, 357–365.

SUPPORTING INFORMATION

Additional supporting information may be found online in the Supporting Information section at the end of this article.

How to cite this article: Fukushima R, Tsujimori T, Aoki S, Aoki K. Trace-element zoning patterns in porphyroblastic garnets in low-*T* eclogites: Parameter optimization of the diffusion-limited REE-uptake model. *Island Arc*. 2021;30: e12394. https://doi.org/10.1111/iar.12394

Document S1 (Elimination of inclusion effects)

Supporting information for:

Trace-element zoning patterns in porphyroblastic garnets in low-*T* eclogites: Parameter optimization of the diffusion-limited REE-uptake model

Ryo Fukushima[1], Tatsuki Tsujimori[1,2], Shogo Aoki[3,4], Kazumasa Aoki[4]

[1] Graduate School of Science, Tohoku University, Sendai 980-8578, Japan
[2] Center for Northeast Asian Studies, Tohoku University, Sendai 980-8576, Japan
[3] Graduate School of International Resource Sciences, Akita University, Akita 010-8502, Japan
[4] Center for Fundamental Education, Okayama University of Science, Okayama 700-0005, Japan

Corresponding author: Ryo Fukushima
E-mail address: ryo.fukushima.p7@dc.tohoku.ac.jp
Address: Graduate School of Science, Tohoku University, 41 Kawauchi, Aoba, Sendai 980-8578, Japan
Phone/Fax: +81-22-795-6236

Journal: Island Arc

```
##THIS IS FOR SYROS SAMPLE

data1 <- read.table("syros.csv",header = T, sep =",")
mat1 <- as.matrix(data1)

delta_x <- 5 * 10^(-4)## cm
xmin <- 1
xmax <- 1333
x <- seq((xmin), (xmax), by = 1)
realx <- delta_x * x

mat2 <- cbind(realx, mat1[,1:29])#data with x axis

######################### removing omp, Jd, zircon, apatite, sphene, rutile######

for(i in xmin:xmax){

  if(mat2[i,"Na23"] > 1000){
    mat2[i, "Na23"] <- NA
  }

  if(mat2[i,"Zr90"] > 1000){
    mat2[i, "Zr90"] <- NA
  }

  if(mat2[i,"P31"] > 10000){
    mat2[i, "P31"] <- NA
  }

  if(mat2[i,"Ti49"] > 3000){
    mat2[i, "Ti49"] <- NA
  }


}
######################### stoichiometric calculation and garnet identification######
thres1 <- 0.2##cations/SiO2 = 1 +- thres1
thres2 <- 0.8##SIO2/Al2O3 = 3 +- thres2

stoic <- matrix(0, nrow=xmax, ncol=5)
for(i in xmin:xmax){
  stoic[i,1] <- (mat2[i, "Ca44"] / 56.08) + (mat2[i, "Mg24"] / 40.30) + (mat2[i, "Fe56"] / 71.84) + (mat2[i, "Mn55"] /
70.94)
  stoic[i,2] <- mat2[i, "Si29"] / 60.08
  stoic[i,3] <- mat2[i, "Al27"] / 101.96

 if(stoic[i,2] == 0){
   stoic[i,4] <- NA
 }
 if(stoic[i,3] == 0){
   stoic[i,5] <- NA
 }
 if(stoic[i,2] != 0 && stoic[i,3] != 0){
   stoic[i,4] <- stoic[i,1] / stoic[i,2]
   stoic[i,5] <- stoic[i,2] / stoic[i,3]

   if(abs(stoic[i,4] - 1) > thres1){
     stoic[i,4] <- NA
   }
   if(abs(stoic[i,5] - 3) > thres2){
     stoic[i,5] <- NA
   }

 }


}

gattai <- cbind(mat2, stoic)

########### exceptonal removing (maybe a pulse)
for(i in xmin:xmax){
  if(gattai[i, "Mn55"] > 20000){
    gattai[i, "Mn55"] <- NA
  }
  if(gattai[i, "Mg24"] > 30000){
    gattai[i, "Mg24"] <- NA
  }
  if(gattai[i, "Ca44"] > 200000){
    gattai[i, "Ca44"] <- NA
```

```
  }
}
############ creating regressed matrix
gattai_reg <- na.omit(gattai)
mat_reg <- gattai_reg[,1:30]### including only garnet points

########### rim definition
for(i in 2:nrow(mat_reg)){
  mat_reg[i,1] <- mat_reg[i,1] - mat_reg[1,1]
}
mat_reg[1,1] <- 0
################################################################################
################### rim to rim plot ########################################


####Li7,Na23,Mg24,Al27,Si29,P31,K39,Ca44,
###Ti49,Mn55,Fe56,Sr88,Y89,Zr90,La139,Ce140,
###Pr141,Nd146,Sm147,Eu153,Gd157,Tb159,Dy163,
#Ho165,Er166,Tm169,Yb172,Lu175,Hf178,


  element <- "Mn55"

  #dataREE <- read.table("REE_kansan.csv",header = T, sep =",")
  #matREE<- as.matrix(dataREE)
  #mat_reg[,element] <- mat_reg[,element] * matREE[3,element]

  plot(mat_reg[,1], mat_reg[,element], type="o")
  #RRoutput <- cbind(mat_reg[,1], mat_reg[,element])
  #write.table(RRoutput, "/Users/RyoFukushima/Desktop/RRoutput.txt", quote = F, row.names = F, col.names = F, append = F)

#############################################################################

############# center identification and creating core-rim plot ##############################
centerx <- 0.287##cm
mat_reg_CR <- mat_reg

for(i in 1:nrow(mat_reg_CR)){
  if(mat_reg_CR[i,1] < centerx){
    mat_reg_CR[i,1] <- NA
  }
}

mat_reg_CR <- na.omit(mat_reg_CR)

for(i in 2:nrow(mat_reg_CR)){
  mat_reg_CR[i,1] <- mat_reg_CR[i,1] - mat_reg_CR[1,1]
}
mat_reg_CR[1,1] <- 0

plot(mat_reg_CR[,1], mat_reg_CR[,element], type="o")
#CRoutput <- cbind(mat_reg_CR[,1], mat_reg_CR[,element])
#write.table(CRoutput, "/Users/RyoFukushima/Desktop/CRoutput.txt", quote = F, row.names = F, col.names = F, append = F)

################################################################################
################################################################################
##THIS IS FOR GUATEMALA SAMPLE

data1 <- read.table("gua.csv",header = T, sep =",")
mat1 <- as.matrix(data1)

delta_x <- 5 * 10^(-4)## cm
xmin <- 1
xmax <- 1549
x <- seq((xmin), (xmax), by = 1)
realx <- delta_x * x

mat2 <- cbind(realx, mat1[,1:29])#data with x axis

######################### removing omp, Jd, zircon, apatite, sphene, rutile######

for(i in xmin:xmax){

  if(mat2[i,"Na23"] > 1000){
    mat2[i, "Na23"] <- NA
  }

  if(mat2[i,"Zr90"] > 1000){
    mat2[i, "Zr90"] <- NA
  }
```

```
  if(mat2[i,"P31"] > 10000){
    mat2[i, "P31"] <- NA
  }

  if(mat2[i,"Ti49"] > 3000){
    mat2[i, "Ti49"] <- NA
  }


}
########################## stoichiometric calculation and garnet identification######
thres1 <- 0.2##cations/SiO2 = 1 +- thres1
thres2 <- 0.8##SIO2/Al2O3 = 3 +- thres2

stoic <- matrix(0, nrow=xmax, ncol=5)
for(i in xmin:xmax){
  stoic[i,1] <- (mat2[i, "Ca44"] / 56.08) + (mat2[i, "Mg24"] / 40.30) + (mat2[i, "Fe56"] / 71.84) + (mat2[i, "Mn55"] /
70.94)
  stoic[i,2] <- mat2[i, "Si29"] / 60.08
  stoic[i,3] <- mat2[i, "Al27"] / 101.96

  if(stoic[i,2] == 0){
    stoic[i,4] <- NA
  }
  if(stoic[i,3] == 0){
    stoic[i,5] <- NA
  }
  if(stoic[i,2] != 0 && stoic[i,3] != 0){
    stoic[i,4] <- stoic[i,1] / stoic[i,2]
    stoic[i,5] <- stoic[i,2] / stoic[i,3]

    if(abs(stoic[i,4] - 1) > thres1){
      stoic[i,4] <- NA
    }
    if(abs(stoic[i,5] - 3) > thres2){
      stoic[i,5] <- NA
    }

  }


}

gattai <- cbind(mat2, stoic)

########### exceptonal removing (maybe a pulse)

for(i in xmin:xmax){
  if(gattai[i, "Mn55"] > 50000){
    gattai[i, "Mn55"] <- NA
  }
  if(gattai[i, "Mg24"] > 40000){
    gattai[i, "Mg24"] <- NA
  }

}

############ creating regressed matrix
gattai_reg <- na.omit(gattai)
mat_reg <- gattai_reg[,1:30]### including only garnet points

########### rim definition
for(i in 2:nrow(mat_reg)){
  mat_reg[i,1] <- mat_reg[i,1] - mat_reg[1,1]
}
mat_reg[1,1] <- 0
################################################################################
#################### rim to rim plot ########################################


####Li7,Na23,Mg24,Al27,Si29,P31,K39,Ca44,
###Ti49,Mn55,Fe56,Sr88,Y89,Zr90,La139,Ce140,
###Pr141,Nd146,Sm147,Eu153,Gd157,Tb159,Dy163,
#Ho165,Er166,Tm169,Yb172,Lu175,Hf178,


element <- "Mn55"

#dataREE <- read.table("REE_kansan.csv",header = T, sep =",")
```

```
#matREE<- as.matrix(dataREE)
#mat_reg[,element] <- mat_reg[,element] * matREE[3,element]

plot(mat_reg[,1], mat_reg[,element], type="o")
#RRoutput <- cbind(mat_reg[,1], mat_reg[,element])
#write.table(RRoutput, "/Users/RyoFukushima/Desktop/RRoutput.txt", quote = F, row.names = F, col.names = F, append = F)

##########################################################################

############# center identification and creating core-rim plot ##############################
centerx <- 0.3265##cm
mat_reg_CR <- mat_reg

for(i in 1:nrow(mat_reg_CR)){
  if(mat_reg_CR[i,1] < centerx){
    mat_reg_CR[i,1] <- NA
  }
}

mat_reg_CR <- na.omit(mat_reg_CR)

for(i in 2:nrow(mat_reg_CR)){
  mat_reg_CR[i,1] <- mat_reg_CR[i,1] - mat_reg_CR[1,1]
}
mat_reg_CR[1,1] <- 0

plot(mat_reg_CR[,1], mat_reg_CR[,element], type="o")
#CRoutput <- cbind(mat_reg_CR[,1], mat_reg_CR[,element])
#write.table(CRoutput, "/Users/RyoFukushima/Desktop/CRoutput.txt", quote = F, row.names = F, col.names = F, append = F)
```